Progress in Oceanography 146 (2016) 1–21

Contents lists available at ScienceDirect

Progress in Oceanography

journal homepage: www.elsevier.com/locate/pocean

Environmental and biological factors controlling the spring phytoplankton bloom at the Patagonian shelf-break front – Degraded fucoxanthin pigments and the importance of microzooplankton grazing

José I. Carreto [a,*], Nora G. Montoya [a], Mario O. Carignan [a], Rut Akselman [a], E. Marcelo Acha [a,b,c], Carla Derisio [a,b]

[a] Instituto Nacional de Investigación y Desarrollo Pesquero (INIDEP), V. Ocampo 1, B7602HSA Mar del Plata, Argentina
[b] Consejo Nacional de Investigaciones Científicas y Técnicas (CONICET), Argentina
[c] Instituto de Investigaciones Marinas y Costeras (IIMyC), Facultad de Ciencias Exactas y Naturales, Universidad Nacional de Mar del Plata, Argentina

ARTICLE INFO

Article history:
Received 16 September 2015
Received in revised form 12 April 2016
Accepted 12 May 2016
Available online 18 May 2016

ABSTRACT

The aim of this study was to investigate the biotic and abiotic factors controlling the spring phytoplankton blooms at the Patagonian shelf-break front (PSBF). Using a CHEMTAX analysis of HPLC pigment data and other methods, the biomass and spatial variability of plankton communities were studied in four sections (39–48°S) across the PSBF during October 2005. Environmental factors and the biomass and composition of plankton communities exhibited a marked spatial heterogeneity. The latitudinal and cross-shelf progression in the timing of the spring bloom initiation and the nutritive properties of the water masses (Subantarctic Shelf Waters and Malvinas Current Waters) seemed to be the key factors. Three plankton regions were distinguished: (a) Outer shelf (OS), (b) Shelf-break front (SBF) and (c) Malvinas Current (MC). At the highly stratified OS region, the post-bloom community showed low-biomasshigh-phytoplankton diversity formed mainly by small cells (haptophytes 30–62%, diatoms 17–49%, chlorophytes 0–34%, and prasinophytes 0–21% of total Chl *a*). High amounts of degraded fucoxanthin were found associated with the heterotrophic dinoflagellate, *Protoperidinium capurroi*. Grazing by this microheterotroph on the diatom population seemed to be the most important factor for the spring bloom decay at the OS. A remarkable *quasi* monospecific bloom (~90%) of a nanodiatom (*Thalassiosira bioculata* var. *raripora*) associated with high Chl *a* (up to 20 mg m^{-3}) occurred along (~1000 km) the SBF and in the most northern extension of the MC. In the southern region, the bloom was developed under absent or incipient density stratification, increasing solar irradiance, high nitrate and phosphate availability, and low numbers of phytoplankton grazers. The average mixedlayer PAR irradiance (<2.0 mol quanta PAR m^{-2} d^{-1}) and Si:N ratios (<0.2) were low, suggesting a diatom population limited by light and under progressive silicate limitation. The more stratified northern region of the SBF showed a later stage of the bloom development, but the large population of diatoms under Si limitation was not in senescence and losses from microzooplankton grazing were minor. The observed high proportion of Chl *a* below a shallow upper mixed layer (up to 85%) could directly reach the bed, favoring the development of epibenthic communities and the formation of seed diatom banks and organic iron-rich sediments. The upwelling along the SBF provides a large source of macronutrients and probably the dissolved iron needed to sustain the intense diatom bloom, but also diatom resting stages that could act as seeds for the next spring bloom. The macronutrient-rich MC region showed low chlorophyll (Chl *a* < 0.8 mg m^{-3}) and a highly diverse phytoplankton community, mainly composed of small cells (diatoms 20–70%, haptophytes 20–40%, chlorophytes 2–25%, prasinophytes 2–18%, and cryptophytes 3–12% of total Chl *a*).

1. Introduction

The Argentine Sea is characterized by the presence of several oceanographic fronts associated with high chlorophyll concentrations (Carreto et al., 1986, 1995, 2007; Piola et al., 2000; Acha et al., 2004, 2015; Bianchi et al., 2009). At the shelf-break, the

* Corresponding author at: Instituto Nacional de Investigación y Desarrollo Pesquero (INIDEP), Paseo Victoria Ocampo N°1, B7602HSA Mar del Plata, Argentina. Tel.: +54 223 486 2586/1292; fax: +54 223 486 1830.
E-mail address: jcarreto@inidep.edu.ar (J.I. Carreto).

http://dx.doi.org/10.1016/j.pocean.2016.05.002
0079-6611/

cooler and more saline waters of the Malvinas Current (MC), which is derived from the Antarctic Circumpolar Current, meet the Subantarctic Shelf Waters (SASW) producing the Patagonian shelf-break front (PSBF) (Carreto et al., 1995; Acha et al., 2004; Matano et al., 2010; Piola et al., 2010). This front is a remarkable ecosystem of significant regional and global importance, recognized as a strong seasonal CO_2 sink associated with highly productive shelf waters (Schloss et al., 2007; Bianchi et al., 2009) and important fishery resources (Bertolotti et al., 1996; Acha et al., 2004, 2015;Wang et al., 2007; Alemany et al., 2009, 2014).

Along the shelf-break consistent streaks of high satellite-chlorophyll concentrations, derived from several ocean color sensors, have been observed during austral spring and summer, often more than 1000 km long (Podestá, 1988; Bertolotti et al., 1996; Saraceno et al., 2005;Rivas et al., 2006; Romero et al., 2006; Signorini et al., 2006, 2009; García et al., 2008). Although significant inter-annual variability in satellite-chlorophyll concentrations is well documented, the mechanisms that drive this variability are not entirely understood (Matano and Palma, 2008; Signorini et al., 2009; Piola et al., 2010). Fieldwork suggests that the development and sustainability of phytoplankton blooms are associated with the supply of nutrients to the surface, especially nitrate and ironfrom the turbulent side of the shelf breakfront (MC Waters). On the other hand, water column structure from the more stratified side of the front (SASW) will affect the light field (Carreto et al., 1995, 2007; García et al., 2008; Signorini et al., 2009). Analytical and numerical results (Matano and Palma, 2008; Matano et al., 2010; Miller et al., 2011)show that the exchange intensity across the front and the associated upwelling increase with an increase in MC transport, the slope of the continental margin, and the friction with the seabed. However, there are limited datasets available to address questions dealing with the underlying mechanistic questions, such as the role and the origin of upwelling along the PSBF (Matano and Palma, 2008; Matano et al., 2010; Miller et al., 2011; Combes and Matano, 2014), or the importance of intrusions of the MC onto the shelf (Piola et al., 2010). To a large extent, this limitation arises from the scarcity of *in situ* observations (Combes and Matano, 2014).

It is known that at the core of this frontal system the phytoplankton blooms begin in the northern region during early austral spring. They are dominated either by diatoms (Carreto et al., 1995; Ferreira et al., 2013; Segura et al., 2013), diatoms and dinoflagellates (García et al., 2008; Akselman and Negri, 2012), or occasionally by dinoflagellates only, which produce brownish-red discoloration patches near the surface (Negri et al., 1992; Akselman and Negri, 2012; Akselman et al., 2014). As can be expected, due to the high latitudinal range of the frontal region, there is a marked difference in timing of the spring bloom initiation and phytoplankton succession, which progresses in a southward direction following a typical pattern associated with the increasing solar radiation and temperature (Rivas et al., 2006; Carreto et al., 2007). At the bloom onset, field estimations of daily water-column integrated primary production were high, but showed a large spatial variability (Schloss et al., 2007; García et al., 2008; Lutz et al., 2010).

A decrease in Chl *a* concentrations is observed during summer, when incident solar irradiance reaches its annual maximum and the mixed layer depth (MLD) is at a minimum. It is accompanied by a shift in the phytoplankton community to a dominance of coccolithophorids (Gayoso, 1995; Signorini et al., 2006; Garcia et al., 2011; Balch et al., 2014), mainly by the low-calcite-containing B/C morphotype of *Emiliania huxleyi* (Poulton et al., 2011, 2013; De Souza et al., 2012) and occasionally *Gephyrocapsa oceanica* (Negri et al., 2003).

Despite the ecological and biogeochemical relevance of the PSBF, to date *in situ* measurements of the prevailing environmental conditions during the period of initiation and development of the spring phytoplankton bloom, which determine the structure of the phytoplankton community, are scarce (García et al., 2008; Segura et al., 2013). In addition, the evaluation of the importance of microplankton and zooplankton grazing in controlling biomass accumulation and phytoplankton species composition arealmost unexplored (Ramirez, 2007; Akselman and Negri, 2012).

A pigment chemotaxonomic approach based on HPLC pigment analysis (Garrido et al., 2011; Jeffrey et al., 2011) remains a useful and powerful technique for distinguishing the main algal groups, especially of the small-sized phytoplankton (Higgins et al., 2011; Kozlowki et al., 2011). In addition, some Chl *a* derivatives formed during senescence may be useful as field signals of phytoplankton cell death and are present in increased abundance during the later stages of bloom development (Walker and Keely, 2004; Szymczak-Zyla et al., 2008; Franklin et al., 2012). Moreover, the spatial heterogeneity in the distribution of Chl *a* and carotenoid transformation products can reflect local variations in the dominant grazing processes (Repeta and Gagosian, 1984; Goericke et al., 1999; Chen et al., 2002).

The aim of this work was to investigate the biotic and abiotic factors controlling the spring phytoplankton blooms at the Patagonian shelf-breakfront. Using a CHEMTAX analysis of HPLC pigment data and other methods, the biomass and the spatial variability of plankton communities were studied in four sections (39–48°S) across the PSBF during October 2005.

2. Material and methods

2.1. Sample collection

Sampling was conducted in four sections across the PSBF (Fig. 1) during early spring (October 8–17, 2005) aboard the R.V. "Puerto Deseado" (GEF-1 cruise). Temperature and salinity profiles were determined using a Sea-Bird 911 CTD (Sea-Bird Electronics, Inc.,

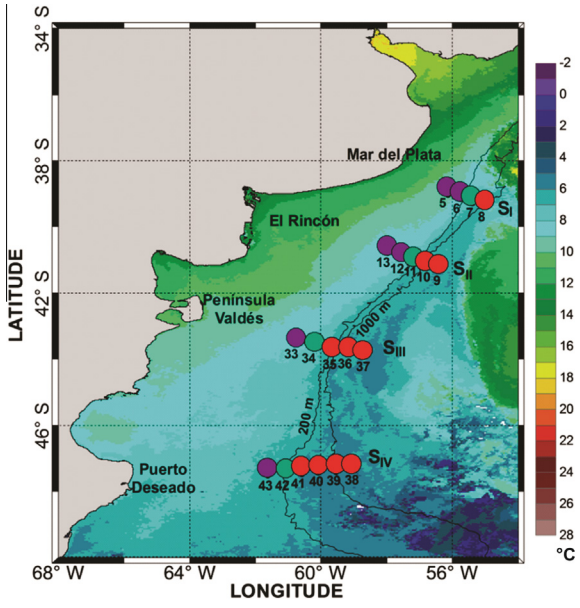

Fig. 1. Surface water masses across sampling stations over the Patagonian shelf-break during the survey, superimposed on a composite (October 8–15, 2005) of a MODIS-Aqua temperature image (°C): Subantarctic shelf water (33.6–33.8; violet circle), Patagonian shelf-break water (33.8–33.9; green circle), and Malvinas Current water (>33.9; red circle). Selected bathymetric contours are indicated. (For interpretation of the references to colour in this figure legend, the reader is referred to the web version of this article.)

U.S.A.). Salinity was determined on board. Salinity samples were collected in 200-mL glass flasks and salinity was determined with a Guildline Autosal 8400B salinometer. The quasi-continuous vertical conductivity-temperature-depth (CTD) profile data and underway surface temperature and salinity data collected during the GEF Patagonia cruises, were reported by Charo and Piola (2014). These data sets are available at the National Oceanographic Data Center, NOAA, U.S.A., http://dx.doi.org/10.7289/V5RN35S0.

In vivo active fluorescence was measured along the ship track by a Model 10-005R Turner Designs fluorometer (Turner U.S.A.), connected to a flow-through system (pumping water from the subsurface ~3.5 m depth). Surface water samples (0 m depth) for the determination of nutrients, pigments, and phytoplankton abundance were collected with a clean plastic bucket. Discrete sampling of the water column was carried out using Niskin bottles attached to a CTD rosette. Seawater samples (0.5–3 L) for pigment determination were filtered under dim light conditions through Whatman™ GF/F glass fiber filters. Filters were frozen immediately in liquid nitrogen (−196 °C) to prevent pigment modification and stored in an ultra-freezer (−86 °C) until analysis once at the laboratory. Water samples for the measurement of nutrients were also frozen in liquid nitrogen and preserved at −86 °C. Water subsamples for the quantitative analysis of phytoplankton were preserved with neutral Lugol's iodine. Additional qualitative samples were collected with a Hensen net (25-μm mesh aperture) and fixed with formaldehyde. Zooplankton were sampled with a Motoda net (60-cm mouth diameter and 200-μm mesh aperture) mounted with a closing mechanism (Motoda, 1969). Tows were performed obliquely within two strata below and above the depth of maximum fluorescence (or selected depths when the water column was homogeneous). Filtered volumes were estimated by employing a digital flowmeter mounted in the sampler. Samples were preserved with 5% formaldehyde.

2.2. Mixed layer depth

The definition of MLD is a subjective matter with numerous criteria commonly in use (De Boyer Montégut et al., 2004 and references therein). In this study, the upper MLD was operationally defined as the depth where σ_t increased by 0.05 kg m^{-3} compared to σ_0 at 5 m depth. We chose the 5 m level to avoid near-surface errors frequently recorded by quasi-continuous CTD instruments.

2.3. Optical parameters

Photosynthetically active radiation (PAR, 400–700 nm) was monitored at the surface continuously during the whole cruise with a cosine downwelling irradiance (LI-COR) sensor. PAR downwelling attenuation coefficients (Kd (PAR) were calculated by Lutz et al. (2010) following the parameterization proposed by Sathyendranath and Platt (1988). The accuracy of the parameterization used was tested for nine stations where *in situ* profiles of irradiance (Iz) were measured using a Biospherical PUV-500/510B radiometer; the average coefficient of variation between the modeled and measured values of Kd (PAR) was 15% ± 8% (Lutz et al., 2010). In some additional stations Kd (PAR) was calculated using an empirical relationship between the calculated/tested Kd and the surface Chl *a* concentration ($R = 0.958$; Sd = 0.017). The euphotic zone depth (Ze) was defined as the depth where irradiance was 1% of surface values.

The critical depth (Zcr) (Sverdrup, 1953) was calculated following the reformulated equation of Nelson and Smith (1991):

$$Zcr = Ed_{[0]}/3.78\ Kd$$

where $Ed_{[0]}$ is the surface PAR irradiance and the coefficient 3.78 is the result of a series of transformations, including a 20% surface PAR reduction due to surface reflectivity, but equivalent to $Ed_{[0]}$ in units of mol quanta m^{-2} day^{-1}. Kd is in units of m^{-1} and Zcr in m.

The average mixed layer PAR irradiance ($Ed_{[ML]}$) was calculated following Poulton et al. (2011) using a combination of $Ed_{[0]}$, Kd, and the MLD as:

$$Ed_{[ML]}\ (\text{mol quanta PAR m}^{-2}\text{d}^{-1}) = Ed_{[0]} \times (1 - \exp^{-Kz})/Kz$$

where Kz = Kd × MLD. $Ed_{[ML]}$ describes the mean light experienced by a particle being mixed from the surface to the base of the mixed layer.

2.4. Nutrient analysis

Frozen (−86 °C) water samples were analyzed for dissolved inorganic nutrients, specifically nitrite, nitrate, phosphate, and silicate using a Technicon TA II Autoanalyzer following the methodologies described in Grasshoff et al. (1983).

2.5. Pigment analysis and data processing

Pigments were extracted with 100% methanol by ultrasonic treatment (Vibra Cell, Sonic and Materials) at 0 °C. The extracts were filtered through GF/F filters to remove cell debris. Water was added to the extract immediately before injection (Jeffrey and Wright, 1997) to obtain an 80% methanol dilution. Sample solution aliquots were automatically injected into an HPLC system Shimadzu LC 10 AC. For pigment elution, we used the method of Zapata et al. (2000). A C8 column (symmetry, 150–4.6 mm, 3.5 μm particle size, 100 A pore size) was used protected with a C8 (Symmetry) guard column. The mixing chamber and column were maintained at 25 °C with a CTO-10 AC (Shimadzu) column oven. Mobile phases were: (A) methanol:acetonitrile:aqueous pyridine solution (0.25 M, pH adjusted to 5.0 with acetic acid) (50:25:25, v/v/v), and (B) methanol:acetonitrile:acetone (20:60:20, v/v/v). A linear gradient from 0% to 40% B was pumped for 22 min, followed by an increase to 95% at minute 28 and an isocratic hold at 95% B for a further 10 min. Peak detection was carried out using a diode array detector (SPD-M10Avp). Chlorophylls were also detected by fluorescence: excitation at 440 and emission at 650 nm (spectral-fluorometer FR-10Axl). Pigments were identified by their retention time and absorption spectra obtained from the online diode array detector (350–750 nm). The HPLC system was calibrated using genuine standards from VKI (The international Agency for ^{14}C Determination, Denmark). Fucoxanthin derivatives were tentatively identified by their polarity and absorption spectra, and quantified using the calibration coefficient of fucoxanthin.

The contribution of different phytoplankton groups to the total Chl *a* at each sampled station were calculated using CHEMTAX, a matrix factorization program running under MATLAB (Mackey et al., 1996). All diagnostic pigments detected, as well as those ambiguous markers indicative of only a few groups, were included in the program matrix (Carreto et al., 2008). A matrix using initial pigment: Chl *a* ratios derived from the studied monospecific diatom bloom (fucoxanthin/Chl *a* = 0.62, chlorophyll c_2/Chl *a* = 0.16, and chlorophyll c_1/Chl *a* = 0.05), supplemented by regional (Carreto et al., 2003, 2008) and global mean field observations (Higgins et al., 2011) was used.

2.6. Plankton analysis

Phytoplankton species were enumerated using an inverted microscope (IX70 Olympus) equipped with epifluorescence and differential interference contrast, with which cell observations on recently fixed cells were also performed. Zooplankton samples were analyzed in the laboratory using a stereoscopic microscope

(Leica S8 APO). Adult and juvenile stages (copepodite IV–V) of copepods were classified to species and all other zooplankton taxa were only enumerated. Taxonomic identification was primarily based on Ramírez (1970a, 1970b, 1971) and Boltovskoy (1981). Zooplankton abundance, expressed as individuals per volume (ind. m^{-3}) was determined for each depth. To analyze the general pattern of copepod horizontal distribution, the data from two depths at the same sampling station were averaged. The copepod community analysis was performed with those species present at least 10% of the stations.

2.7. Remote-sensing

Sea surface temperature (SST) and chlorophyll were obtained from data collected from the Aqua Moderate-resolution Imaging Spectroradiometer (MODIS-Aqua) at a 4-km resolution (8 day composites), and from data collected from the SeaWiFS and processed to level 3. All data were obtained from the Ocean Color Website (http://oceancolor.gsfc.nasa.gov).

3. Results

3.1. Hydrography

During the sampling period, the temperature and salinity data showed the presence of SASW (33.6–33.8), MCwater (MCW: >33.9) and the transition between these two water types: the Patagonian shelf-break waters (PSBW) (Fig. 1) (Guerrero and Piola, 1997; Piola and Rivas, 1997; García et al., 2008; Painter et al., 2010). The transition from SASW to MCW is depicted by the 33.8–33.9 isohalines, which, on average, are located just offshore of the 200 m isobath (Romero et al., 2006; Matano et al., 2010; Piola et al., 2010). We used the position of the 33.9 isohaline to indicate the position of the shelf-break front (SBF) and the separation between SASW and MCW (Romero et al., 2006).

Salinity distribution in section I (S_I) showed (Fig. 2) a frontal boundary with strong vertical inclination. The result is that surface waters with salinities ranging from 33.8 to 33.9 occupy a large geographical area offshore of the shelf-break. *In situ* observations, numerical models, and recent satellite observations showed a significant transfer of a mixture of SASW and Río de la Plata waters (RLPW) towards the deep ocean into the Brazil-Malvinas Confluence (BMC) region (approximately 36°S). However, the contribution of the Río de la Plata discharge during the spring is quantitatively insignificant (Matano et al., 2010, 2014; Guerrero et al., 2014; Strub et al., 2015).

Our results showed that the exportation of shelf waters towards the deep ocean can also be significant at 40°S (S_I). Sections towards the south (S_{II}, S_{III}) revealed that the sharp transition at the surface between SASW and MCW were localized inshore of the shelf-break, overlyingthe 120–150 m isobaths. In S_{III}, the strong intrusion of MCW into the shelf is accompanied by the upward displacement of high salinity (34.1), low temperature (<4 °C), and high nutrient waters (Figs. 2 and 5), indicating the upwelling of deep nutrient rich MCW near the shelf-break. In the more austral section (S_{IV}), the slope of the continental marginis less abrupt (see isobath separations in Fig. 1) and consequently the intrusion of the MCW onto the shelf (Piola et al., 2010) becomes more weak, so that the relaxed SBF (as indicate by the 33.9 isohaline) closely follows the 200 m isobath. Temperature and density sections (Fig. 2) showed a similar structure to the corresponding salinity sections. However, temperature sections also showed a marked latitudinal decrease in both surface temperature and thermal stratification, following the typical pattern associated with the southward increase of solar radiation and surface net heat flux (Rivas et al., 2006). In addition, S_{II} showed a minimum surface temperature near the SBF that appeared to be produced by the displacement of shallow water

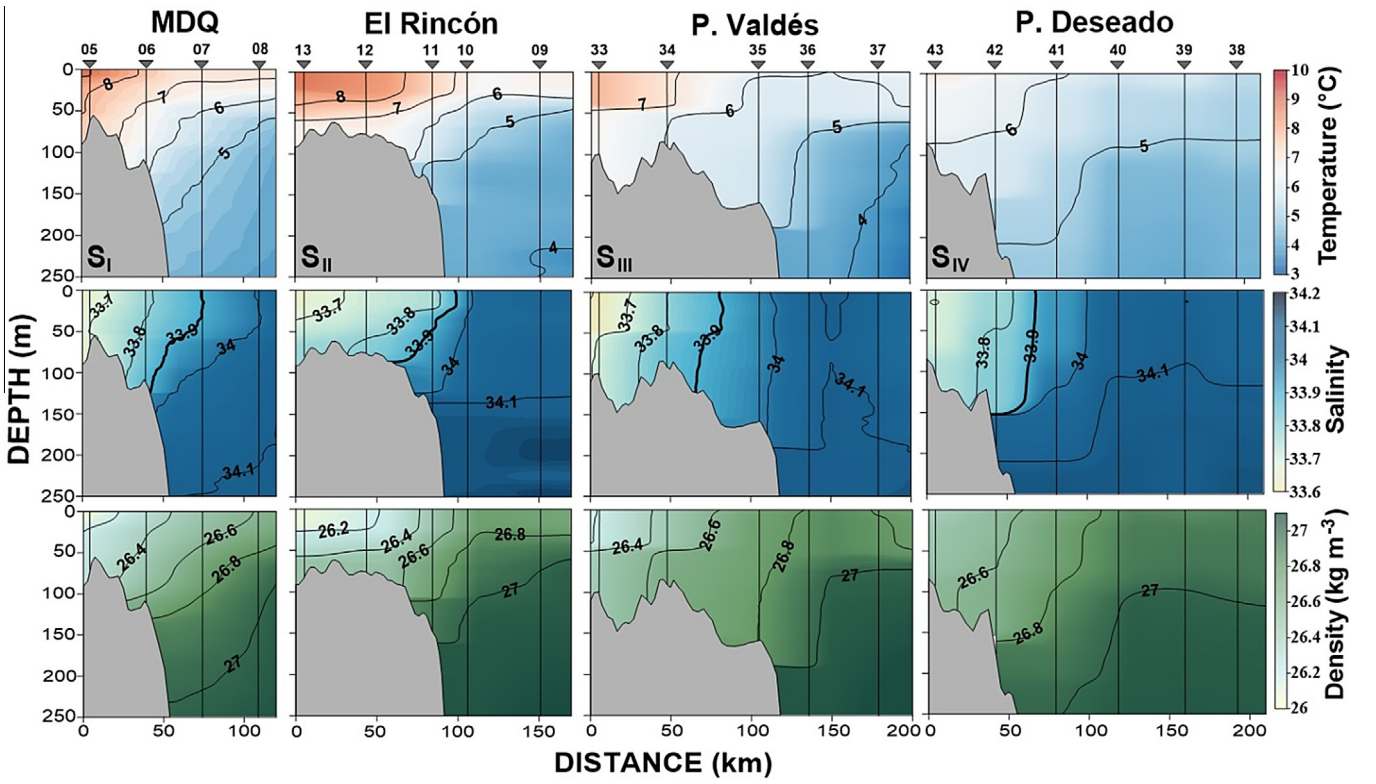

Fig. 2. Water column distribution of temperature (upper panel), salinity (medium panel), and density (lower panel), in the studied sections. Station numbers are marked at the top of the graph. Mar del Plata denoted as MDQ.

to the surface. This finding may suggest a weak and localized upwelling at the front at this location. Nevertheless, recent studies have shown that the MC also tends to organize itself in the form of jets of colder water, separated by narrow, relatively warm, slower bands (Piola et al., 2013; Combes and Matano, 2014). Satellite sea surface temperature data (Fig. 1) showed the occurrence of several discontinuities and intermittent areas of lower temperature compared to the surrounding waters, indicating the heterogeneity of the MC.

3.2. Mixed layer depth, critical depth, and euphotic zone depth

The MLD was <100 m along the four study sections, and was deeper in the southern section than in the northern section (Fig. 3). MLDs were typically <35 m northward and >35 m southward of 42°S, dividing the data set into two groups: S_I and S_{II} versus S_{III} and S_{IV}. CTD data show a mean MLD of 23 m (11–31 m)for the northern group and 58 m (15–98 m) for the southern one (Fig. 3).

In the northern sections (S_I and S_{II}), the differences in thickness of the ML between the shelf, the slope, and the oceanic stations were small. Although the lower values of the MLD were found at the inner shelf stations (St5 = 11 m; St13 = 15 m), there was no significant negative relationship with bottom depth, since the highest values of the MLD were found in the frontal region (St7 = 33 m; St10 = 29 m) and not at the oceanic stations. Differences in the MLDs were very marked along the southern sections (S_{III} and S_{IV}). In S_{III}, the water column near the slope presented the lowest stratification, as the MLD was much deeper (St35 = 97 m) than that observed, both at the shelf (St33 = 42 m; St34 = 45 m) and at the oceanic stations (St36 = 58 m; St37 = 47 m). A more complex situation was observed in S_{IV}, where, in addition to the transition between the shelf (St43 = 15 m) and the slope MLD (St42 = 72 m), a second and more intense discontinuity was observed between adjacent oceanic stations (St39 = 20 m; St38 = 98 m). At all stations, the Zcr closely followed the Ze and was consistently deeper than the Ze, which ranged from 15 (St7) to 35 m (St6) (Fig. 4). In the more stratified northern section, Ze was similar to the MLD (St5 to St13), although minor differences among inner (St5, St6, and St13) and frontal stations (St7) were evident. Differences were very marked in the southern sections (Fig. 4). With the exceptions of St39 and St43, the MLD was very much deeper than both the Ze and the Zcr. However, Zcr and MLD were very close at stations 34 and 37 (Fig. 4).

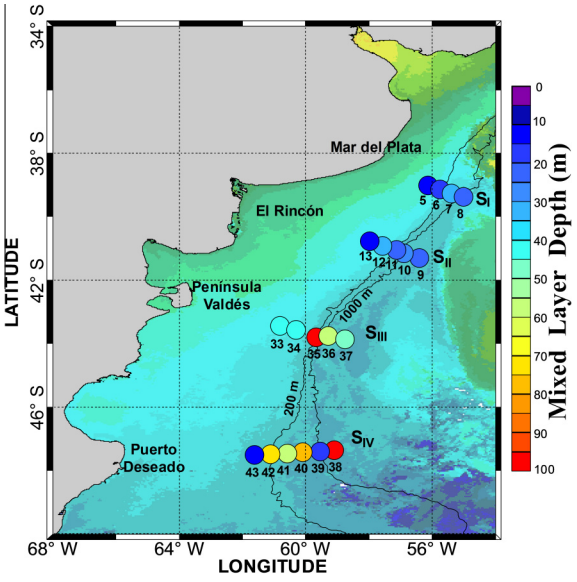

Fig. 3. Mixed layers depths (MLDs) as calculated using the threshold criteria of 0.05 σ_t, superimposed on a composite (October 8–15, 2005, Fig. 1) of MODIS-Aqua temperature (°C) images.

3.3. Nutrient distributions

Nutrient concentrations at the surface (Table 1; Fig. 5) followed an inverse latitudinal gradient to temperature, with the high surface nitrate, phosphate, and silicate concentrations in the more austral section (S_{IV}), that generally decline northwards in both the shelf-break and MCW. Vertical nutrient distributions were related to temperature of the water masses. The lowest nutrient concentrations (approximately 1–2 μM nitrate, 0.3–0.4 μM phosphate, and 1–2 μM silicate) were observed in the surface waters of St 7, in association with the highest Chl *a* levels (Figs. 5 and 6). Nutrient concentrations were also relatively low in the stratified most northern location (St8) of the MC, whereas section III showed a marked positive gradient between the outer shelf (OS) and the oceanic MCW (Fig. 5). The nitrate concentrations in the OS waters were also relatively low, but a sharp increase in nitrate concentration was observed near the shelf-break, being more intense in section III, probably due to the upwelling of MCW (Fig. 5).

In the more austral section (S_{IV}) the nutrient front relaxed and high surface nitrate and phosphate concentrations were observed in both the OS and the MCW (Fig. 5). The large stock of nitrate and phosphate in these surface layers suggest that, at this time, they are only slightly consumed by the phytoplankton activity. However, the association between high Chl *a* (St41 > 15.0 mg m^{-3}, Fig. 6) and low silicate concentrations in the euphotic zone (~1 μM) suggest that silicate could be the limiting nutrient for diatom growth. The vertical distribution of this nutrient was similar to that described for nitrate, but the surface concentration gradient from the OS to the MCW was less marked. At the surface, silicate concentrations varied from 1 to 6 μM, increasing with depth in a similar pattern to that of nitrate. However, silicate increased more slowly with depth and continued to increase almost all the way to the bottom oceanic waters (results not shown).

Near the surface the Si:N ratios were variable (0.14–1.27), but generally lower than one. The highest value was observed in the most northern extension of the MC(S_I), near the BMC in association with the surface Chl *a* maximum (Fig. 6). Ratios lower than one (Si:N ~ 0.48) were also observed in the deep waters (300–500 m) of the MC., indicating that in Subantactic waters, silicate is the limiting macronutrient for diatom growth. A notable trend in N:P ratios was observed along the frontal region. Within surface bloom waters (0–30 m) the lowest N:P ratio was 3.7 and was found in the northern section, coinciding with the Chl *a* maxima (Fig. 6). Although this relationship generally increased with latitude, within the diatom bloom band the highest values (N:P = 20.1) were found at the vertically mixed St35 (Fig. 3). A similar trend was observed in the MC surface waters, having N:P ratios between 13.8 at the northern St8 and 18.8 at the more austral St38.

3.4. Chlorophyll a distribution

The surface Chl *a* concentrations derived from the SeaWiFS imagery and obtained from *in situ* data, showed the same general distributional pattern (Fig. 6). In both cases, data revealed a band of high Chl *a* concentrations along the shelf-break front, extending northwards from 50°S up to 39°S, where the chlorophyll maximum (20 mg m^{-3}) was found.

The vertical concentrations of Chl *a* in the studied sections are shown in Fig. 6. Section$_I$ shows that the high concentrations of Chl *a* (>16 mg m^{-3}) observed eastward of the shelf-break (St7) were distributed homogeneously within the mixed layer

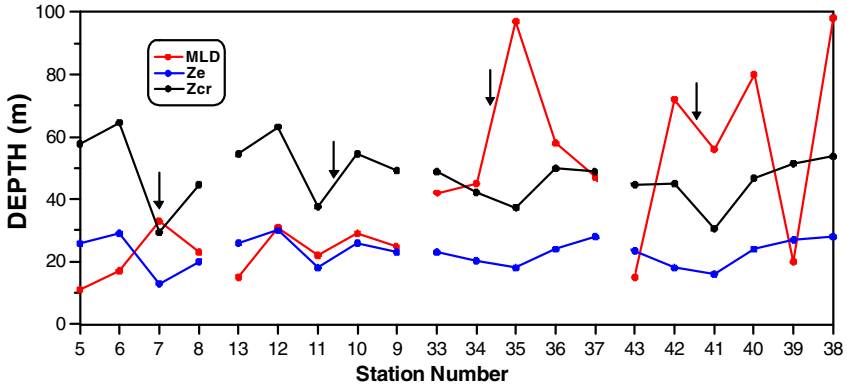

Fig. 4. Mixed layer depth (MLD, red), euphotic zone depth (Ze, blue) and Sverdrup critical depth (Zcr, black). Arrows indicate the position of the shelf-break front (salinity 33.9). (For interpretation of the references to colour in this figure legend, the reader is referred to the web version of this article.)

Table 1
Values of surface water chemical properties and chlorophyll *a* concentration at all stations along the Patagonian shelf-break in October 2005: SST, sea surface temperature: SSS, sea surface salinity; NO_3^-, nitrate; PO_4^{-3}, phosphate; SiO_3^{-2}, silicic acid.

Station ID	Date (October 2015)	Latitude (°S)	Longitude (°W)	Water depth (m)	SST (°C)	SSS	NO_3^- (μM)	PO_4^{-3} (μM)	SiO_3^{-2} (μM)
5	9	−39.008	−56.135	85	9.20	33.64	5.23	0.71	2.35
6	9	−39.137	−55.766	125	8.07	33.77	6.43	0.61	2.60
7	9	−39.261	−55.406	770	7.15	33.86	1.42	0.45	1.53
8	9	−39.380	−55.027	1100	7.16	34.04	6.05	0.55	0.98
9	10	−41.298	−56.422	1529	6.77	34.07	6.22	0.45	0.80
10	10	−41.146	−56.908	970	6.49	34.07	10.01	0.51	2.04
11	10	−41.049	−57.125	120	7.96	33.76	3.18	0.36	1.75
12	10	−40.912	−57.581	79	8.35	33.72	4.38	0.78	2.33
13	10	−40.770	−57.988	86	8.93	33.65	3.06	0.29	1.07
33	15	−43.443	−60.812	98	7.95	33.59	1.25	0.75	1.04
34	15	−43.569	−60.317	103	7.08	33.81	3.70	0.52	1.48
35	15	−43.798	−59.672	150	6.34	33.96	9.15	0.50	1.57
36	15	−43.755	−59.291	1327	5.99	34.12	13.40	0.77	3.12
37	16	−43.865	−58.765	1940	6.35	34.02	12.66	0.96	5.03
38	16	−47.369	−59.097	1570	5.27	34.05	17.39	0.90	6.83
39	17	−47.395	−59.545	994	5.82	34.05	16.11	0.92	5.03
40	17	−47.427	−60.102	678	5.56	34.08	14.30	0.68	2.52
41	17	−47.459	−60.597	451	6.08	33.94	7.91	0.33	1.14
42	17	−47.494	−61.119	144	6.59	33.79	5.28	0.52	0.80
43	17	−47.516	−61.615	135	7.46	33.71	6.65	0.58	1.08

(MLD = 33 m), then slightly decreased with depth but remained high (5.64 mg m^{-3}) at a depth of 80 m. The more oceanic station (St8, MLD = 23 m) also showed high Chl *a* concentrations homogeneously distributed from the surface (4.41 mg m^{-3}) to close to 50 m depth (6.38 mg m^{-3}). The lowest Chl *a* concentrations (<1.0 mg m^{-3}) were observed at the western side of the shelf-break. In S_{II}, the highest concentration of Chl *a* (19.9 mg m^{-3}) was observed at the western side of the shelf break (St11) below the MLD (22 m). This station also showed high concentrations of Chl *a* (5.9 mg m^{-3}) down to 80 m depth. At the shelf-break (St10) and at the most oceanic station (St9), the Chl *a* concentrations were relatively high in the upper layer (4.1 and 2.1 mg m^{-3}, respectively), but decreased markedly below the MLD. The lowest Chl *a* concentrations (0.16–0.06 mg m^{-3}) were observed in the OS, near the western border of the bloom (St12). In S_{III} high concentrations of Chl *a* were found in the OS (St34; Chl *a* ~7 mg m^{-3}), the shelf-break(St35; Chl *a* ~10 mg m^{-3}) and the MCW (St36; Chl *a* ~3 mg m^{-3}). At the shelf-break where the mixed layer was very deep (97 m) the high concentration of Chl *a* observed at the surface, was distributed almost homogeneously in the water column, slightly decreasing up to 80 m depth (5.2 mg m^{-3}).

A similar vertical distribution was observed at St36, whereas in St34 (MLD = 45 m), at the western side of the chlorophyll maximum, the high Chl *a* concentrations (>7 mg m^{-3}) were restricted to the upper layer (~30 m). Minor concentrations of Chl *a*, were found at the extreme stations of the section located in the shelf (St33 = 0.7 mg m^{-3}) and oceanic domains (St37 = 0.4 mg m^{-3}). $Section_{IV}$ also showed an extended bloom across the SBF (Fig. 6), involving the OS (St42), the shelf break (St41) and the MCW (St40). Surface layer Chl *a* concentrations were similar for St41 and St42 (8.11 and 9.7 mg m^{-3}, respectively). However, whereas in the water column of St42 (MLD = 72 m) Chl *a* concentrations were distributed almost homogeneously, at St41 (MLD = 56 m) the largest concentration (17.8 mg m^{-3}) was present at the subsurface (25 m). As at other sections, the low Chl *a* characteristic of the more oceanic MC stations (St38 and St39), was homogeneously distributed in the water column. At the western extreme of this transect, the low surface concentrations of Chl *a* (<1.0 mg m^{-3}) at St43 sharply increased (>4.0 mg m^{-3}) at the subsurface (20 m).

As can be expected, the highest integrated (100 m deep) Chl *a* values were observed at S7 (1162 mg m^{-2}), St11 (967 mg m^{-2}), St35 (794 mg m^{-2}) and St41 (849 mg m^{-2}). In these bloom stations, most of the phytoplankton biomass was distributed below the euphotic zone, indicating a progressive limitation of light with depth during the growth period, which can be partially alleviated by the effect of vertical mixing (Figs. 7a and 4).

At the more stratified northern region (St7 and St11), a large fraction of the phytoplankton biomass is located below the MLD (Fig 7a).

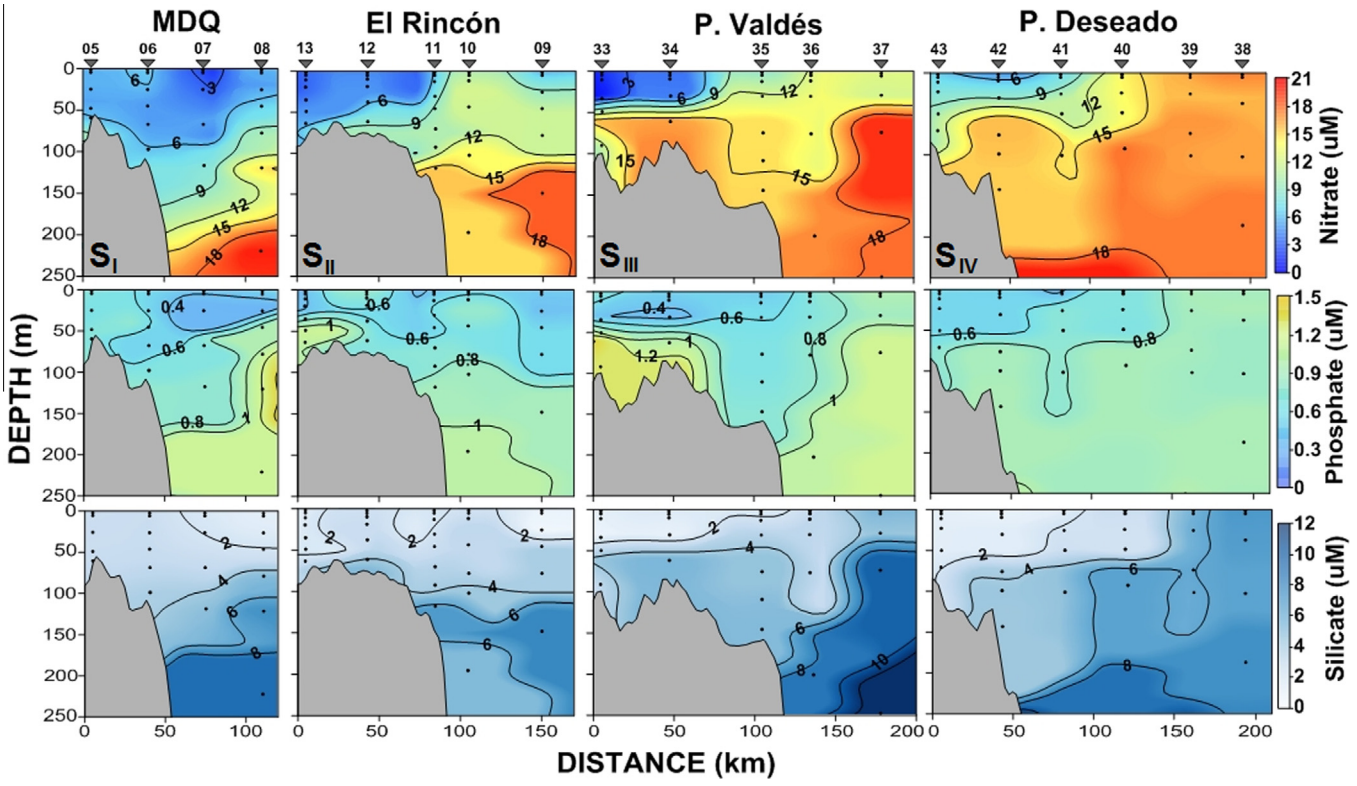

Fig. 5. Water column distribution of nitrate (μM), phosphate (μM), and silicate (μM) in the corresponding sections. Station numbers are marked at the top of the graph. Mar del Plata denoted as MDQ.

Average mixed layer PAR irradiance ($Ed_{[ML]}$) (Fig. 7b) was generally low (<6.7 mol quanta PAR $m^{-2}\,d^{-1}$), being lower (4.2 mol quanta PAR $m^{-2}\,d^{-1}$) in the southern (S_{III} and S_{IV}) than in the northern (S_I and S_{II}) sections (9.2 mol quanta PAR $m^{-2}\,d^{-1}$). This latitudinal contrast is related to the differences in the MLD among these regions (Fig. 4). However, in both regions, the lowest $Ed_{[ML]}$ values in each section were observed at the stations showing the highest integrated Chl *a* biomass (St7, St11, St35, and St41) (Fig. 7a and b).

3.5. Pigment pattern and abundance of algal groups

Based on the obtained pigment patterns (HPLC data available as Supplementary Data) and previous results on phytoplankton species composition (Ferrario, 2008; Sabatini et al., 2012; Segura et al., 2013;Ferrario et al., 2013), three principal phytoplankton communities closely related to the hydrography of the area were distinguished as follows: (a) the shelf-break bloom community, (b) the high nutrient low chlorophyll (HNLC) MC community, and (c) the post-bloom northern OS community. As an example, the selected ($n = 95$) HPLC chromatograms of pigment extract from three surface samples (St35, 0 m; St6, 0 m; St37, 0 m) show the characteristic pigment patterns that prevailed in the phytoplankton assemblages considered (Fig. 8 and Table 2).

Fucoxanthin (Fuco) was by far the most abundant carotenoid in the overall area of the shelf-break front, being particularly high (up to 13.8 mg m^{-3}) at the maximum Chl *a* concentrations observed in this region (St7, 11, 35, 41, and 42). Chl c_2 and Chl c_1 were the major Chl *c* pigments, whereas Chl c_3, MVChl c_3 and MgDVP were present only in minor concentrations. Traces of 19′-hexanoiloxyfucoxanthin (Hex-fuco) and peridinin (Peri) were only detected in some samples. The microscopic analysis of these samples (Ferrario, 2008; Sabatini et al., 2012; Ferrario et al., 2013; Segura et al., 2013) indicated that the phytoplankton community was mainly comprised of nanoplanktonic (8.5–12 μm) diatoms, explaining the observed abundance of Fuco, Chl c_1 and Chl c_2 (Diatoms pigment type-1; Diatoms PT-1). In addition, the presence of minor amounts of Chl c_3 and the absence of other pigments markers of haptophytes (e.g. Hex-fuco), indicate the occurrence of other types of diatom species (Diatoms pigment type-2; Diatoms PT-2) containing these pigments (Jeffrey et al., 2011).

Microscopy revealed that various species of *Pseudo-nitzschia* and *Chaetoceros* were secondary components of the diatom assemblage (Ferrario, 2008; Sabatini et al., 2012). As expected from pigment analysis, the relative contribution of the various groups to Chl *a* calculated by CHEMTAX (Fig. 9) showed that along the shelf-break front, diatoms were the dominant group (>90% of total Chl *a*). Moreover, diatoms prevailed along the entire sampled water column (Fig. 10). The main component of this diatom community (Diatoms PT-1) was identified by Ferrario et al. (2013) as *Thalassiosira bioculata* var. *raripora*, which reached concentrations of up to 4.5×10^3 cells mL^{-1} and at some stations represented more than 90% of total phytoplankton abundance. At the highest Chl *a* concentration (19.6 mg m^{-3}) attained at St7, the Diatoms PT-1 group represented 98.2% of total Chl *a*.

Diatoms were also relatively abundant (30–70% of total Chl *a*) components of the HNLCMC community (St37, 38, and 39), but in this case the contribution of Diatoms PT-2 (up to 56% of total diatoms) was relatively more important than in the shelf-break bloom community (Fig. 9). Nevertheless, the presence of major unequivocal pigment markers indicated that the phytoplankton diversity in this low biomass assemblage (Chl $a = 0.12$ to 1.03 mg m^{-3}) was higher than that observed in the SBF assemblage. The pigment data showed that in addition to Fuco, MVChlc_3, Chlc_3, But-fuco, and Hex-fuco were also present. Hex-fuco was the dominant acyl-fucoxanthin, indicating that the contribution of

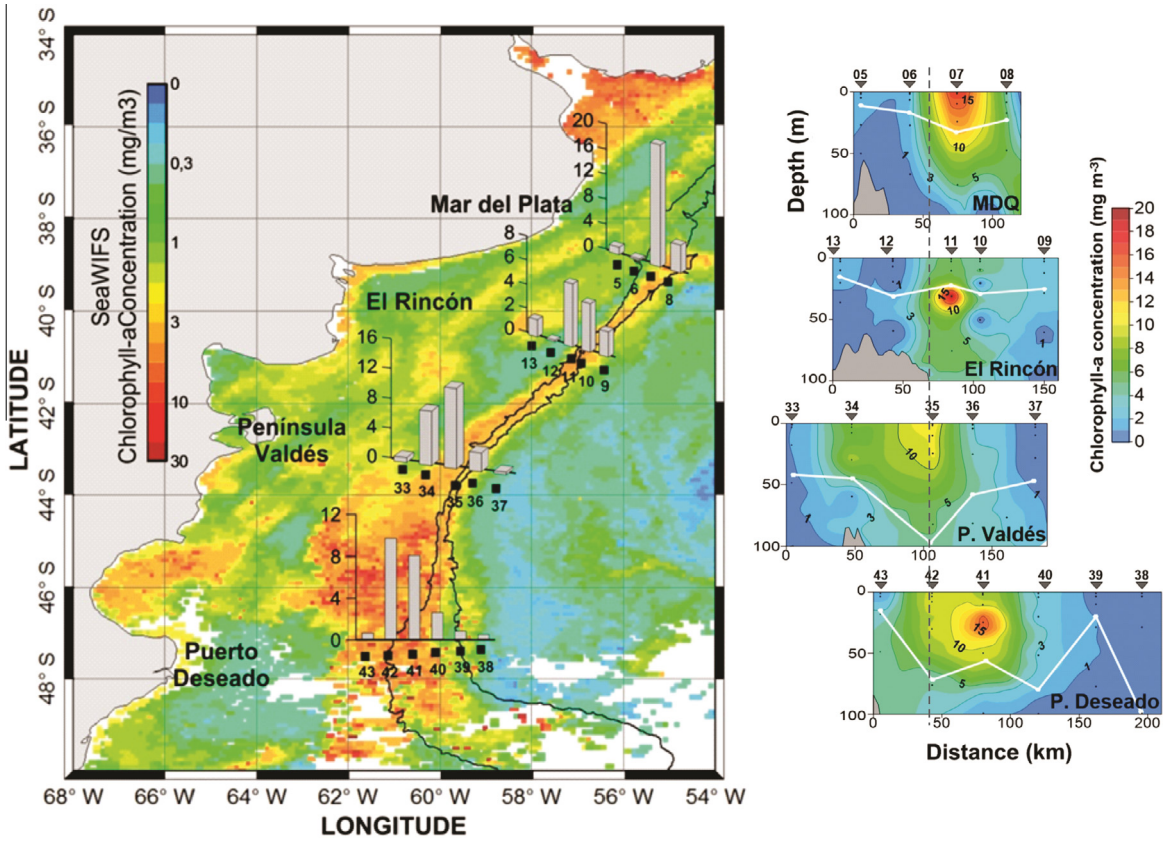

Fig. 6. Left panel: SeaWiFS chlorophyll image composite from October 8–15, 2005, showing the high chlorophyll band along the Patagonian shelf-break and the *in situ* surface Chl *a* concentrations (vertical bars, mg m^{-3}) at the sampling stations (October 8–17, 2005). Bathymetric lines as in Fig. 1. Right panel: Water column distribution of Chl *a* (mg m^{-3}) in the four studied sections. The white line connects the mixed layer depths calculated for each station. Station numbers are marked at the top of each graph. Mar del Plata denoted as MDQ.

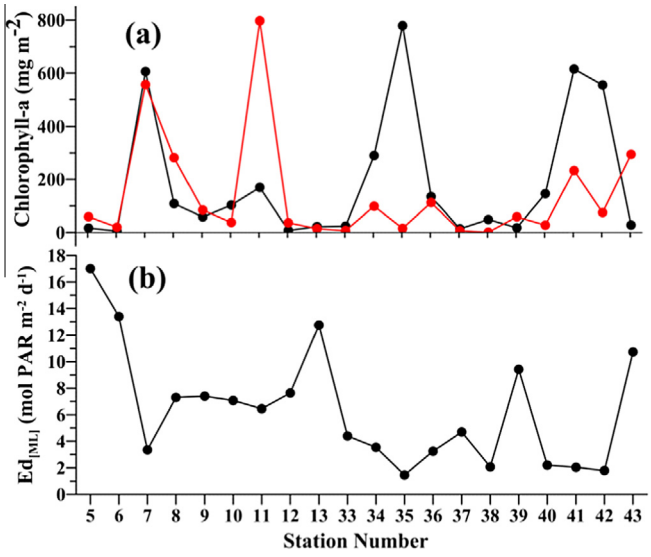

Fig. 7. (a) Integrated Chl *a* (mg m^{-2}) in the mixed layer depth (dark circle) and below the mixed layer depth (red circle). (b) Average mixed layer PAR irradiance ($Ed_{[ML]}$). (For interpretation of the references to colour in this figure legend, the reader is referred to the web version of this article.)

haptophytes to the total Chl *a* could be important. The CHEMTAX results (Figs. 9 and 10) indicate that their contribution to total Chl *a* varied between 20% and 40%. The presence of the additional useful marker pigments, $Chlc_2$-MGDG [18/14] and $Chlc_2$-MGDG [14/14] indicate the occurrence of a complex haptophyte population containing different pigment groups (Zapata et al., 2004; Carreto et al., 2008; Jeffrey et al., 2011). The relative contribution of these haptophyte-types to total Chl *a* calculated by CHEMTAX (Fig. 9) showed that species of the *Phaeocystis*-PT8 group (7–14%) and *Chrysochromulina*-PT7 group (1–14.5%) were the more relevant members among this community. Microscopy also showed the presence of *Emiliania huxleyi* (Ferrario, 2008; Segura et al., 2013), but our estimated contribution of *Emiliania*-PT6 group to total Chl *a* (Fig. 9) was relatively low (0–5%).

The low biomass-high phytoplankton diversity community of the OS (St5, 6, 12, and 13) showed a similar pigment composition to that described for the HNLC community. However, diatoms were relatively less abundant (17–49% of total Chl *a*) and the contribution of Diatoms PT-2 was more important (up to 100% of total diatoms) than in the HNLC MC community (Figs. 9 and 10). The microscopic analysis of these samples (Segura et al., 2013) indicated that the diatom community was mainly comprised of ultra-planktonic diatoms (<5 μm). In many samples Hex-Fuco was the dominant xanthophyll (Fig. 8), indicating that haptophytes could be relatively abundant in this community. Moreover, the abundance of the other useful haptophyte marker pigments, $Chlc_2$-MGDG [18/14] and Chl c_2-MGDG [14/14] (Zapata et al., 2004; Jeffrey et al., 2011), indicated that a pigment family of haptophytes containing these two non-polar Chls c_2 (*Chrysochromulina*-PT7) was also relatively abundant (Zapata et al., 2004; Carreto et al., 2008; Jeffrey et al., 2011). The relative contribution of these haptophyte-types to total Chl *a* calculated by CHEMTAX (Fig. 9), showed that species of the *Chrysochromulina*-PT7 (2–37%), *Emiliania*-PT6 (0–31%), and *Phaeocystis*-PT8 (7–14%) were all relevant

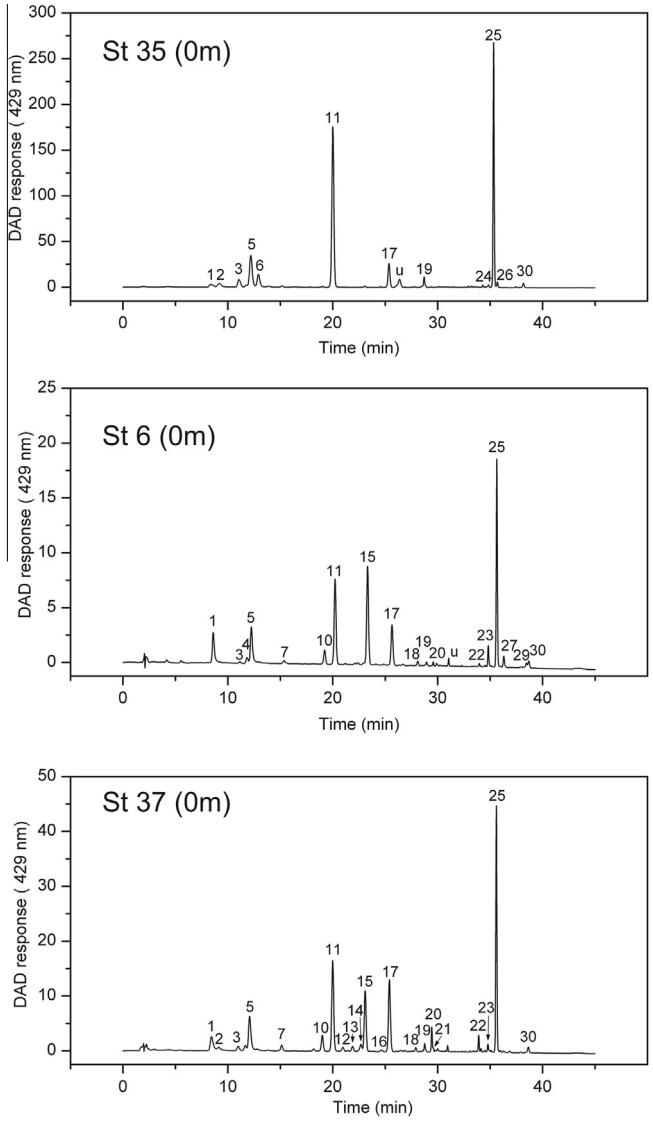

Fig. 8. HPLC chromatograms of pigment extracts from surface samples (0 m depth) of three selected stations representative of the distinguished phytoplankton communities. Detection was by absorbance at 429 nm; peak identification as in Table 2.

members of this community. Microscopy also showed that in addition to *Emiliania huxleyi* and *Chrysochromulina* spp., other unidentified haptophytes were important members of this phytoplankton assemblage (Segura et al., 2013). In addition to the major pigment markers, Pras, Lut, Zea, and Allo were also detected in minor or trace amounts.

The relative contribution of the various groups to the total Chl *a* calculated by CHEMTAX, showed that in contrast to the almost exclusive diatom dominance observed in the shelf-break front, the community of the OS (Figs. 9 and 10) was more complex, mainly formed by small cells. It was principally comprised of haptophytes (30–62%), diatoms (17–49%), chlorophytes (0–34%), prasinophytes (0–21%), and cryptophytes (0–11%), with a small contribution by cyanobacteria (0–6%).

3.6. Remote sensing observations and bloom evolution

The scenario presented in the composite of color images from October 8-15 (Fig. 6) provides a first order impression of the gradients in surface Chl *a* along and across the SBF, during the sampling period. However, as it provides no temporal information on the initiation, development, and bloom decline, an eight-day image composite is presented (Fig. 11) to provide this temporal pattern.

Inspection of this figure reveals a main latitudinal difference in the timing of the spring bloom initiation and development. In this region, the phytoplankton bloom started on the OS in late winter (Fig. 11a). It then expanded to the shelf-break and the adjacent oceanic region in the northern area (St7 and St8), and to the shelf south of 44°S, reaching its maximum development (Fig. 11c) after two weeks. At this time, satellite data reveal a band of high Chl *a* concentrations (~20 mg m^{-3}) along the SBF, extending southward from 38°S up to approximately 47°S. At the time of our research cruise (October 8–15), both the satellite chlorophyll values (Fig. 11e) and those determined *in situ* (Fig. 6), were lower in some places than those observed in the previous weeks (Fig. 11).

The decline of the phytoplankton bloom was very marked in the northern OS region (St5, 6, 12, 13, and 33), where nutrient concentrations no longer seemed to be limiting (see Section 3.2). Further south (44–50°S), the phytoplankton bloom began two weeks later, in early spring (Fig. 13c), mainly following the north-south progression in solar radiation and day length. Thereafter, (October 16–23, 2005) the decline in the bloom seemed to extend to the entire shelf-break and adjacent oceanic region (Fig. 11f).

Table 2
Peak identification and abbreviation pigment name used in the text.

Peak no.	Pigment	Abbreviation
1	Chlorophyll c_3	Chl c_3
2	Monovinyl chlorophyll c_3	MVChl c_3
3	Chlorophyllide *a*	Chlide *a*
4	Mg 2,4-divinylpheoporphyrin a_5 monomethyl ester	MgDVP
5	Chlorophyll c_2	Chl c_2
6	Chlorophyll c_1	Chl c_1
7	Peridinin	Peri
8	Pheophorbide *a*	Pheide *a*
9	Pyropheophorbide *a*	Ppheide *a*
10	19′-Butanoyloxyfucoxanthin	But-fuco
11	Fucoxanthin	Fuco
12	9′-*cis*-neoxanthin	Neo
13	Prasinoxanthin	Pras
14	Violaxanthin	Viola
15	19′-Hexanoyloxyfucoxanthin	Hex-fuco
16	Diadinochrome	Diadchr
17	Diadinoxanthin	Diadino
18	Alloxanthin	Allo
19	Diatoxanthin	Diato
20	Zeaxanthin	Zea
21	Lutein	Lut
22	Chlorophyll *b*	Chl *b*
23	Chlorophyll c_2 monogalactosyl-diacylglyceride ester [18:4/14:0]	Chlc_2-MGDG [18/14]
24	Chlorophyll *a* allomers	Ch *a* allo
25	Chlorophyll *a*	Chl *a*
26	Chlorophyll *a* epimer	Chl *a*′
27	Chlorophyll c_2 monogalactosyl-diacylglyceride ester [14:0/14:0]	Chlc_2-MGDG [14/14]
28	Pheophytin *a*	Phe *a*
29	β,ε-Carotene	β,ε-Car
30	β,β-Carotene	β,β-Car
31	Pyropheophytin *a*	Pphe *a*

3.7. Degraded phytoplankton pigments

At most of the stations studied, only chlorophyllide *a* (Chlide)-not their methyl-ester- was detected in minor amounts (1–5% of Chl *a*), indicating the absence of senescent cells, zooplankton fecal pellets and/or activity of an intracellular chlorophyllase (Jeffrey

Fig. 9. Percentage distribution of the main surface phytoplankton groups contributing to total Chl *a* concentration, as estimated by interpretation of pigment HPLC data using the CHEMTAX program. Note three (0–100%, 0–40%, and 0–25%) scale bar levels.

and Hallegraeff, 1987). Moreover, the presence of Chl *a* allomers (Chl *a* allo) and Chl *a* epimers (Chl *á*) were clearly only detected in the shelf-break diatom bloom samples. Chl *a* concentrations was very high in these samples, allowing the easier recognition of trace (≈1% of total Chl *a*) components. However, HPLC-chromatograms of pigment extracts from samples taken at St33,

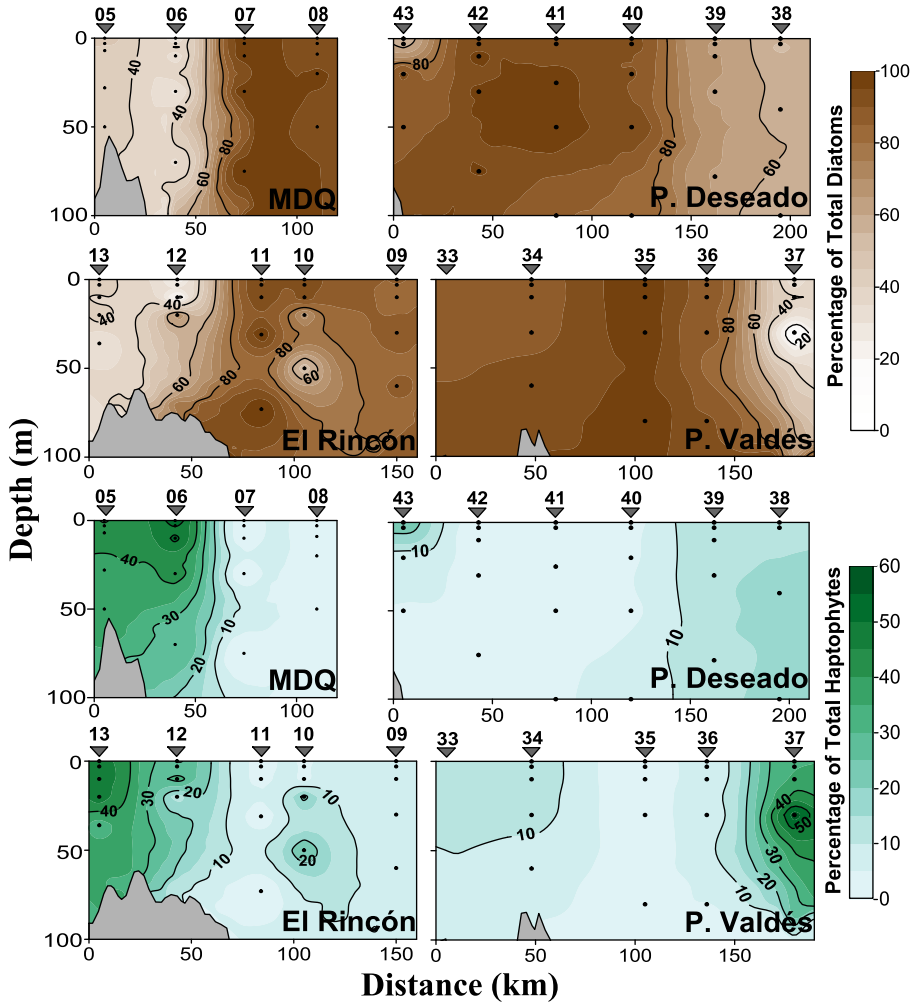

Fig. 10. Percentage vertical distribution of total diatoms (upper panel) and total haptophytes (lower panel) contributing to the total Chl *a* concentration, as estimated by interpretation of pigment HPLC data using the CHEMTAX program, along the studied sections. Station numbers are marked at the top of each graph. Mar del Plata denoted as MDQ.

showed (Fig. 12) that pyropheophorbide *a*, (Ppheide *a*) was present as the main degraded Chl *a* product. Pheophorbide *a* (Pheide*a*), pyropheophytin (Pphe *a*), pheophytin *a* (Phe *a*), Chl *a* allo, and other unidentified cyclic pheophorbides (Harradine et al., 1996; Goericke et al., 1999, 2000; Louda et al., 2011; Franklin et al., 2012; Bale et al., 2015) were also present in minor or trace amounts. Sterol chlorin esters (SCEs) and carotenol chlorin esters (CCEs) were not found. The absence of these copepod grazing biomarkers indicate a minimal input of mesozooplankton feces to the water column (Repeta and Gagosian, 1984; Harradine et al., 1996; Goericke et al., 1999; Chen et al., 2002). Interestingly, the chromatograms showed the presence of high amounts of an unknown carotenoid (F459), accompanied by minor amounts of Fuco, Diadino, Diato, β-β-car, Chl *a*, Chl c_2, Chl c_1, and several non-identified carotenoids (Fig. 12 and Table 2). These findings suggest that the main unknown carotenoid (F459) may be a derivative of Fuco, enzymatically produced by microheterotrophic organisms.

In relation to fucoxanthin, the visible spectrum of the major fucoxanthin derivative (F459) and its *cis*-isomer (c-F459) shows a bathochromic shift of +9 nm (λ_{max} = 459 nm in the HPLC solvent) and a total loss of fine structure (Fig. 12), characteristic of a cross-conjugated carbonyl derivative. Their spectra and chromatographic behavior closely match isofucoxanthinol dehydrate (iso-Fuco-dhy) (Repeta and Gagosian, 1984; Goericke et al., 1999), but we do not have spectroscopic data available to confirm this hypothesis. An unknown carotenoid (P460), with similar absorption spectra but of higher polarity was observed by Ferreira et al. (2013) in several samples taken during the spring at the PSBF. Its presence was associated with the observed shift in the blue peak (440–460 nm) of the *in vivo* phytoplankton spectral absorption of these samples (Ferreira et al., 2013).

The highest concentrations of F459 were measured at the surface of St33 (1.64 mg m^{-3}). Its vertical distribution showed high concentrations (1.64–1.28 mg m^{-3}), almost uniformly distributed in the top 30 m of the water column, then decreasing with depth, but remaining high (0.66 mg m^{-3}) below the MLD (42 m). Conversely, the low surface concentration of c-F459 (0.13 mg m^{-3}) increased with depth, reaching a similar concentration (~0.5 mg m^{-3}) to that of F459 below the MLD (Fig. 13). These results suggest that c-F459 is produced by chemical isomerization of F-459. Furthermore, a large change was observed in the F459: Chl*a* ratio, ranging between 2.2 and 5.6, between the surface layer and the base of the ML, suggesting a relatively greater stability of F459.

Although at low concentration levels, the HPLC methodology employed was unable to completely resolve F-459 from peridinine (Per, λ_{max} = 476 nm), a fine spectral analysis of our chromatograms revealed that in the phytoplankton community of the OS (St6 and St12), F459 and c-F459 were relatively abundant just below the

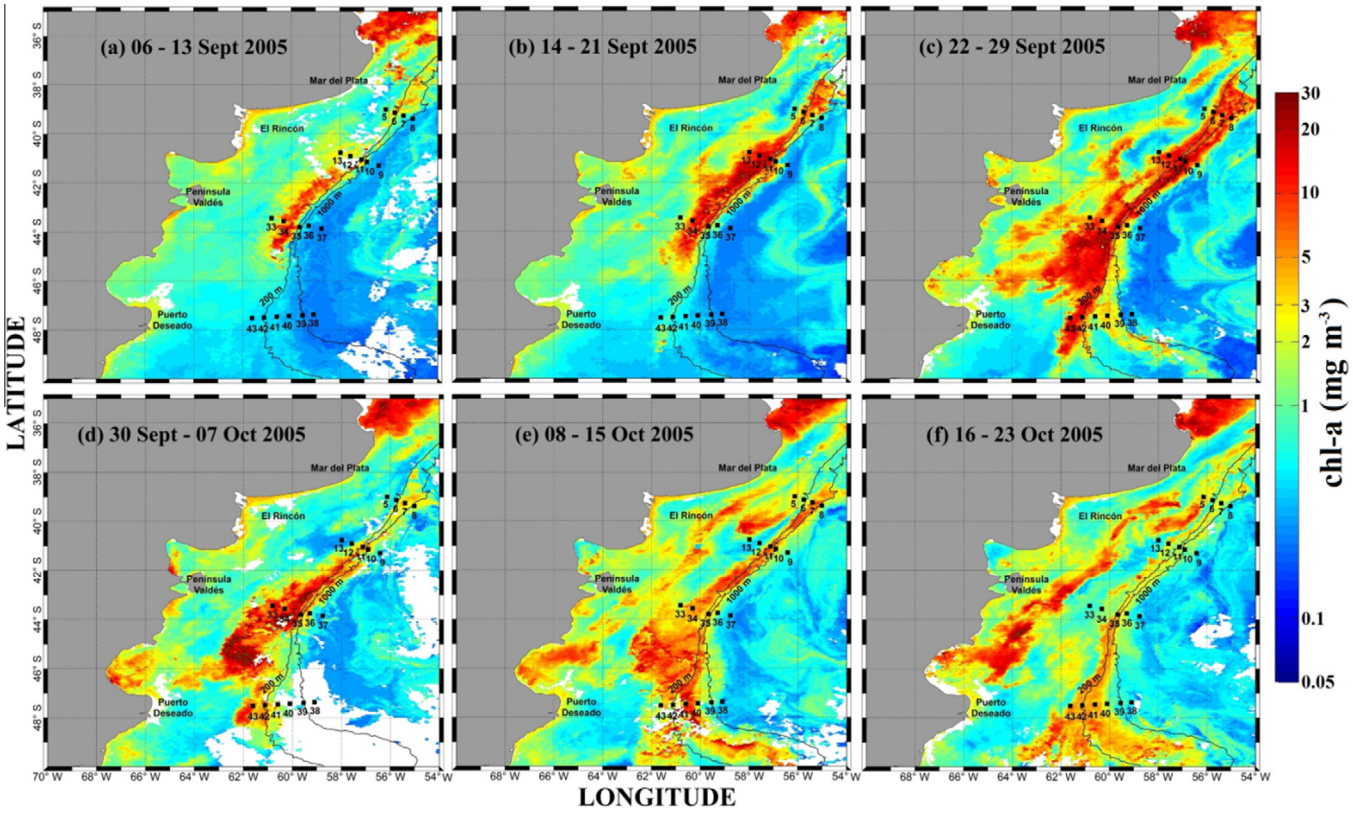

Fig. 11. Eight-day composite of MODIS-Aqua Chl *a* images, during the period September 6 to October 23, 2005. Bathymetric contours as shown in Fig. 1. Sampling was conducted during the period October 8–17, 2005.

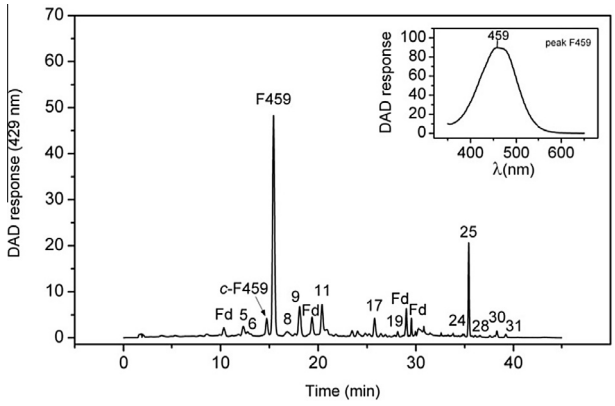

Fig. 12. HPLC chromatogram of pigment extract from surface samples from station 33. Detection was by absorbance at 429 nm; peak number identification as in Table 1. Fd = fucoxanthin derivatives; F459 = iso-Fuco-dhy-like; and c-F459 = their *cis* isomer. The *insert* shows the absorbance spectrum of peak F459.

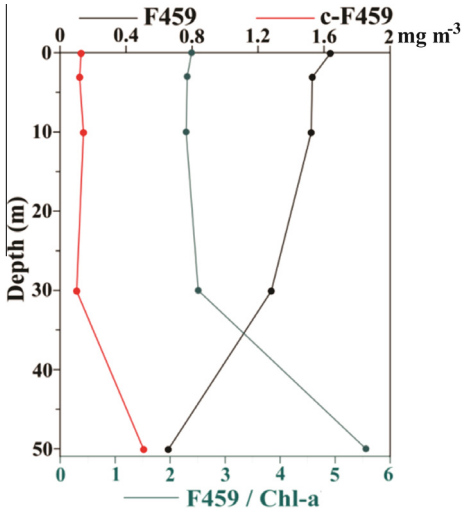

Fig. 13. Vertical distribution of F459 (black circle), c-F459 (red circle) and the F459/Chl *a* ratio (green circle) at St33. (For interpretation of the references to colour in this figure legend, the reader is referred to the web version of this article.)

MLD (F459/Fuco ≈ 1.5). In contrast, at some high-biomass SBF stations (St7, 11, and 34), F-459 was relatively high(Fig. 16b) at the surface (~0.5 mg m^{-3}), though the F459/Fuco ratio was very low (F459/Fuco ≈ 0.05).

3.8. Abundance and distribution of predators

3.8.1. Protozooplankton

The distribution of non-photosynthetic unicellular organisms in the 10–200 μm size fraction, generally displayed its highest values in the western border of the diatom bloom band. Maxima were found in S_{III} (St33 = 27.8 cells mL^{-1} and St34 = 33.0 cells mL^{-1}) in coincidence with the highest concentrations of degraded fucoxanthin (F459) (Figs. 14a and 16b). The lower abundances were found at the northern shelf stations (St5 = 1.1 cells mL^{-1} and St13 = 1.4 cells mL^{-1}) and in the stations of S_{IV}, where values ranged

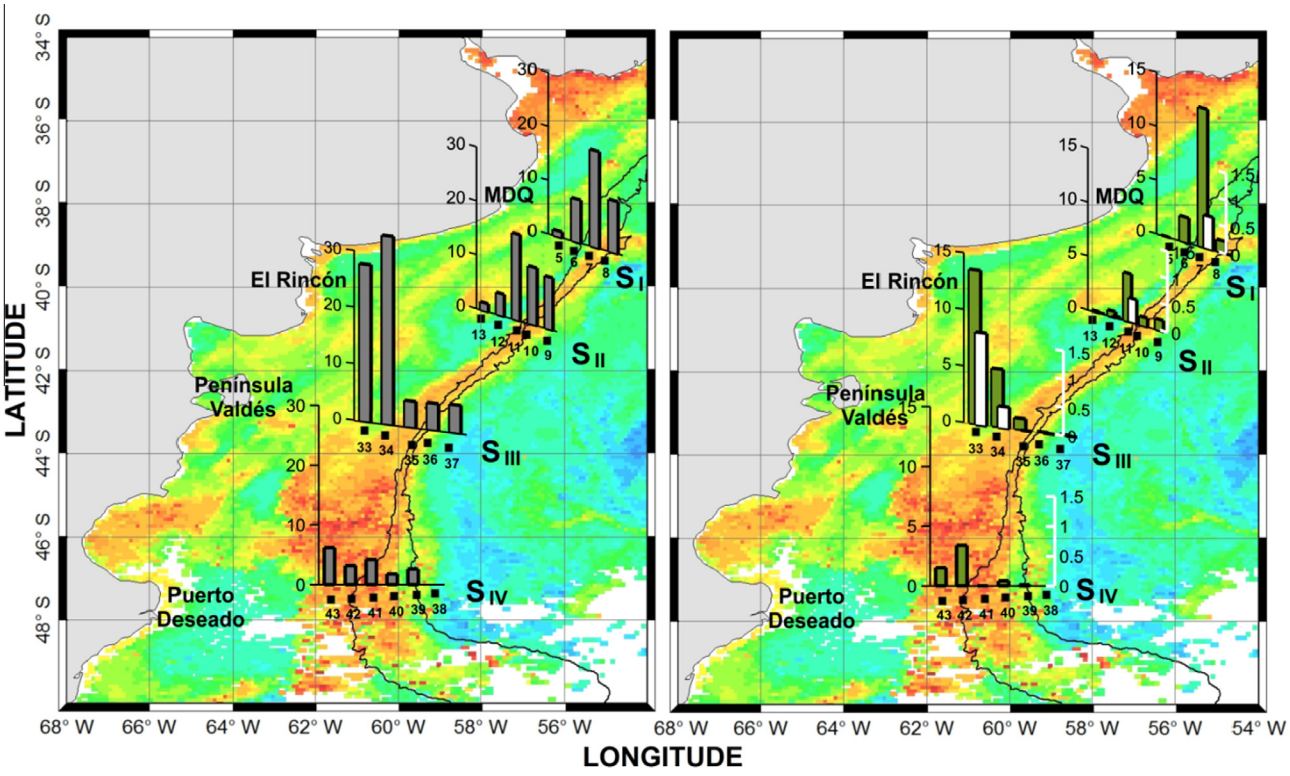

Fig. 14. Distribution and abundance of microheterotrophs and F459 in the studied area during the spring superimposed on composites (October 8–15, 2005) of SeaWiFS chlorophyll images. Left panel: mean water column concentration of nano- and microheterotrophs (cells mL^{-1}, gray bars). Right panel: surface concentration of *Protoperidinium* spp. (cells mL^{-1}, green bars) and F459 (mg m^{-3}, white bars). (For interpretation of the references to colour in this figure legend, the reader is referred to the web version of this article.)

between 1.8 cells mL^{-1} (St40) to 6.2 cells mL^{-1} (St43). The observed latitudinal decline in the abundance of microheterotrophs was probably related to the timing of the spring bloom initiation. By contrast, the paucity observed at the northern shelf stations, appeared to be related to the abundance of the dominant copepod *Oithona atlantica* (Fig. 15).

Dinoflagellates and non-identified flagellates constituted the main taxa of the nanoplanktonic (10–20 μm) heterotrophs, whereas the microplanktonic size range (20–200 μm) showed a net predominance by heterotrophic/phagotrophic dinoflagellates and a minimum abundance of aloricate ciliates. The dinoflagellates *Protoperidinium capurroi*, *P. decens*, *P. vulgare*, *P. punctulatum*, *P. mastophorum*, *P. acanthophorum*, *P. pentagonum*, *Gyrodinium spirale*, *G. fusus*, and species of *Protoperidinium*, *Amphidinium*, and *Oxytoxum*, in addition to other unidentified dinoflagellate species, were the main components of the heterotrophic community associated with the *T. bioculata* var. *raripora* bloom. The abundance of all these non-photosynthetic species were, however, markedly different. *P. capurroi* was widely dominant in most of the samples examined, attaining abundances of up to 12.3 cells mL^{-1} (90.4%). The spatial distribution of the genus *Protoperidinium* displayed its highest values (13.6 cells mL^{-1}) associated with the diatom bloom band that stretched along the shelf-break front. Maxima were found at St33, in coincidence with the highest concentrations (1.64 mg m^{-3}) of degraded fucoxanthin (F459) (Fig. 14b). The lower values appeared both in the low-biomass high-phytoplankton diversity communities of the OS, much as in the MCW. Similar to other species of *Protoperidinium* (Jacobson and Anderson, 1986), *P. capurroi* exhibits the ability to develop a hyaline cytoplasmic extension or feeding veil emitted from the hypocone, and reaching up to twice the length of the cell. The presence of a feeding veil in the *P. capurroi* population was observed to be associated with several recently captured *T. bioculata* var. *raripora* cells at an early stage of digestion (Fig. 15). These observations suggest that F459 was produced as a consequence of the predatory activity of heterotrophic dinoflagellates, *P. capurroi* being the most prevalent species.

Fig. 15. *Protoperidinium capurroi* showing a developed feeding veil (arrow) associated with several recently captured *Thalassiosira bioculata* var. *raripora* cells at an early stage of digestion.

3.8.2. Copepods

The zooplankton biomass during spring was mostly dominated by copepods. However, unlike previous studies (Berasategui et al.,

2006; Ramirez, 2007), we cannot identify a clear pattern in the distribution of dominant copepod species across the SBF, due to the fact that the copepod assemblages of the OS and MCW overlapped. The following species dominated the copepod community, representing 97.7% of the total abundance: *Calanus simillimus*, *Centropagesbrachiatus*, *Clausocalanus laticeps*, *Clausocalanus brevipes*, *Ctenocalanus vanus*, *Drepanopus forcipatus*, *Oithona atlantica,* and *Oithona similis* (syn *O. helgolandica*; Ramírez, 1970a). However, several less abundant or rarely occurring species were also present, mainly at the oceanic stations: *Euchaeta marina*, *Metridia lucens*, *Rhincalanus nasutus*, *Neocalanus tonsus,* and *Eucalanus longiceps*. The most abundant copepod species were typical of shelf waters, but at some offshore stations, a mixture of shelf and oceanic species from MCW were found (Ramírez, 2007).

In contrast to the lack of a spatial pattern in species composition, the numerical results showed marked tendencies in the zooplankton abundance distributions. A remarkable decrease in zooplankton abundance from north to south was evident (Fig. 16). These findings were expected due to the marked difference in timing of the spring bloom initiation, mainly following the north-south progression of water column stabilization (Carreto et al., 2007; Rivas et al., 2006).

The highest abundance of copepods (3800 ind. m^{-3}) was found in the OS of the northern section (St5), where the cyclopoid copepod *Oithona atlantica* was the most abundant species (2400 ind. m^{-3}), along with *Ctenocalanus vanus* (537 ind. m^{-3}) and *Calanus brevipes* (245 ind. m^{-3}) (Fig. 16).

Other species present (*Calanus simillimus*, *Drepanopus forcipatus,* and *Oithona similis*) were much less abundant (Fig. 16). Comparatively, these values are much lower than those previously recorded in this area (3000–7000 ind. m^{-3}) during late spring and early summer (Ramirez, 2007, 1981). The lowest abundance of copepods was found in the more austral $S_{IV,}$ showing values ranging from 0.1 ind. m^{-3} (St43) at the OS to 23.4 ind. m^{-3} in the MC (St38). In this southern section, euphausiid eggs or euphausiid juveniles and adults were more abundant than copepods, mainly over the HNLC area under the influence of the MC (Sabatini et al., 2012). These findings suggest an initial state in the seasonal succession of the mesozooplankton community. The patterns of copepod distribution and abundance, those of their prey (phytoplankton) availability, and especially the distribution and abundance of degraded phytoplankton pigments were weakly matched (Fig. 16), suggesting a poor coupling between consumers and their prey communities.

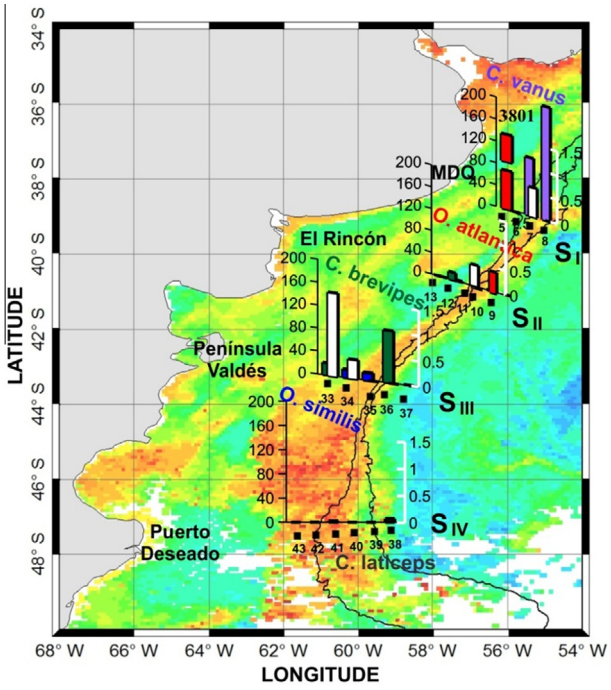

Fig. 16. Mean water column distribution of copepod abundances (ind. m^{-3}; gray scale) and of F459 concentrations (mg m^{-3}; white scale and bars) in the studied area during spring, superimposed on composites (October 8–15, 2005) of SeaWiFS chlorophyll images. Color bars denote the dominant species: red = *Oithona atlantica*, cyan = *Ctenocalanus vanus*, green = *Clausocalanus brevipes*, blue = *Oithona similis*, gray = *Clausocalanus laticeps*. Note that the red bar is not continuous, due to the high abundance (3800 ind. m^{-3}) of copepods. (For interpretation of the references to colour in this figure legend, the reader is referred to the web version of this article.)

4. Discussion

Despite the ecological and biogeochemical relevance of the PSBF, to date, *in situ* measurements of the biotic and abiotic factors controlling the initiation and development of the spring phytoplankton bloom are scarce (Carreto et al., 1995; García et al., 2008; Sabatini et al., 2012). Phytoplankton blooms are periods of rapid growth and accumulation of phytoplankton cells that occur when growth rates exceed loss rates. Phytoplankton growth rates are species-specific (or strain-specific) characteristics, that are modulated by several environmental factors, such as irradiance, water column stability, nutrient supply, and temperature, while losses can occur through predation, advection, vertical mixing, sinking, viral attack, or other forms of mortality. Therefore, the rapid phytoplankton accumulation during the spring bloom must be due to either an alleviation of those factors constraining growth, a reduction in factors determining losses, or (more probably) a combination of both (Daniels et al., 2015).

Satellite images document that during 2005 the spring phytoplankton bloom started at the northern OS during late winter. Thereafter, the bloom expanded to the south and to the east, extending over the SBF and the adjacent oceanic region, reaching its maximum development after two weeks. South of 45°S the phytoplankton bloom begins later, in early spring at the SBF, following the north-south progression in solar radiation and day length. These results are coincident with those obtained in previous monthly color satellite image studies on the Patagonian shelf (Saraceno et al., 2005; Rivas et al., 2006; Romero et al., 2006; Signorini et al., 2009). In accordance with the described spatio-temporal variation, our *in situ* data revealed that several stages of the spring bloom occurred during the cruise. The environment, biomass, and composition of the phytoplankton communities and their potentials predators, therefore exhibited a marked spatial heterogeneity. The latitudinal and the cross-shelf progression in the timing of the spring bloom initiation and the nutritive properties of the water masses at the Patagonian frontal boundary (SASW, MCW, and PSBW) seem to be the main factors determining the observed spatial heterogeneity. Three principal plankton regions related with the stage of bloom evolution, and spatially segregated by the prevailing environmental conditions were distinguished: (a) OS (post bloom community), (b) SBF (bloom community) and (c) MC (HNLC).

4.1. Outer shelf

Because of the time elapsed between the beginning of the sea surface warming triggered by a positive change in the air-sea heat fluxes (Rivas et al., 2006; Smyth et al., 2014) and our sampling, this relatively shallow (~100 m) and low turbulent region occupied by SASW showed a marked thermal stratification. Traditionally, Sverdrup's critical depth hypothesis (Sverdrup, 1953) has been applied to many marine ecosystems with the goal of evaluating the roles of light availability and vertical mixing leading to phytoplankton

spring blooms (Nelson and Smith, 1991; Townsend et al., 1992; Signorini et al., 2009). Our data showed that the thin (<22 m), well illuminated ($Ed_{[ML]}$ = 12–17 mol quanta PAR m^{-2} d^{-1}) mixed layer (ML) was shallower than the light dependent Zcr. Macronutrient concentrations were lower than those observed during the winter period (Carreto et al., 1995), but did not impart any kind of severe limitation (Fig. 5) to the phytoplankton population. The scenario, however, showed low-phytoplankton biomass and high-community diversity, dominated by small cells (haptophytes 30–62%, chlorophytes 0–34%, prasinophytes 0–21% of total Chl *a*), whereas the diatom population (17–49% of total Chl *a*) was mainly comprised of ultra-planktonic (<5 μm) forms (Segura et al., 2013). The haptophytes, *Emiliania huxleyi, Chrysochromulina* spp., and *Phaeocystis* spp. were important members of this phytoplankton assemblage, typical of the spring bloom decay (October–November) described for the Patagonian shelf (Carreto et al., 2008; Gonçalves-Araujo et al., 2012; Poulton et al., 2013). Blooms of the coccolithophore *Emiliania huxleyi* have been regularly observed at the Patagonian shelf, during late spring and summer (Gayoso, 1995; Garcia et al., 2011; Poulton et al., 2011, 2013; De Souza et al., 2012; Balch et al., 2014).

These findings suggest that losses due to grazing pressure could be an important factor controlling the spring bloom decay and the structure of the plankton community in this OS ecosystem. It is recognized that microzooplankton are the most important consumers of phytoplankton, leading to important losses during the spring bloom due to their relatively high abundance and grazing rates compared to copepods (Calbet and Landry, 2004; Jeong et al., 2012; Löder et al., 2011). A global data synthesis (Calbet and Landry, 2004) reported that grazing by microzooplankton can account for 67% of primary production across all marine ecosystem types, and 57% in the coastal ocean. Protists of this size class are also a significant food resource for mesozooplankton (Löder et al., 2011; Scherr et al., 2013; Zamora-Terol et al., 2013) and fish larvae (Montagnes et al., 2010).

In the OS, dinoflagellates and non-identified flagellates constituted the main taxa of nanoplanktonic heterotrophs, whereas the microplanktonic size range showed a net predominance of heterotrophic/phagotrophic dinoflagellates of the *Protoperidinium* genus, and a minimum abundance of aloricate ciliates. The maximum abundance of the *Protoperidinium* genus was found at mid-latitudes in the OS (St33 = 13.6 cells mL^{-1}), associated with a low phytoplankton biomass (Chl *a* = 0.66 mg m^{-3}) and the highest detected concentrations of the main fucoxanthin derivative F459. In addition to F459 and their isomer c-F459, several Chl *a* derivatives (Ppheide, Pheide *a*, Pphe *a*, Phe *a*) were also present, in some cases in minor or trace amounts. Moreover, the copepods grazing biomarkers, SCEs and CCEs were not found (Repeta and Gagosian, 1984; Harradine et al., 1996; Goericke et al., 1999, 2000; Chen et al., 2002; Louda et al., 2011). These facts and the observation of a feeding veil in *P. capurroi* containing several recently captured *T. bioculata* var. *raripora* cells at an early stage of digestion, indicate that F459 was produced by the predatory activity of heterotrophic dinoflagellates, *P. capurroi* being the most prevalent species.

There is growing recognition that heterotrophic dinoflagellates could be the major consumers of diatoms in blooms initiated by a variety of processes, including upwelling, river runoff, iron fertilization, and the arrival of spring (Calbet and Landry, 2004; Scherr and Scherr, 2007). However, the resulting grazing pigment derivatives have hardly been studied (Neveaux and Soyer, 1976; Carreto, 1985).

At St33, the mean concentration of F459 in the top 30 m of the water column was 1.50 mg m^{-3}. This implies (assuming a Fuco/F459 ratio of 1) a consumption of at least 2.5 mg m^{-3} of Chl *a* (Fuco/Chl *a* ratio = 0.60), or 75 mg m^{-2} of Chl *a*. Using F-459 as a grazing biomarker and adopting a C/Chl *a* ratio of 50 (g:g) (Llewellyn and Gibb, 2000), we estimate that the *P. capurroi* population could have consumed 3.75 g C m^{-2} during the period the cruise was conducted. Adopting the measured *Ditylum brightwellii* consumption rate by *P. huberi* (17.8 ngC ind^{-1} day^{-1}) (Buskey et al., 1994; Jeong et al., 2012) as that of *P. capurroi*, and taking into account that total cell numbers of *P. capurroi* in the first 30 m of St33 was 266.1×10^6 cells m^{-2}, our estimate of diatom loss was 4.73 g C m^{-2} day^{-1}. Regarding the maximum photosynthetic carbon assimilation measured at the time of this study (5.48 g C m^{-2} - day^{-1}; Lutz et al., 2010), our estimated losses were high enough to explain the recent decline of the diatom bloom at this station, a process that probably occurred earlier in the northernmost region of the OS. In contrast, at the core of the bloom (see the SBF section below), the lower relative abundance of *P. capurroi* and the low P459/Chl *a* ratio suggest that, in the SBF, especially in the more southern region, microzooplankton grazing was at an early stage of development. These findings support the idea that the spring diatom bloom occurred because physicochemical factors allowed diatoms to initially grow faster than co-occurring microzooplankton, which were food-limited until blooms attained a higher biomass (Calbet and Landry, 2004; Scherr et al., 2013).

It has been recognized that most copepods prefer feeding on microzooplankton, due to their large size, easy perception, and relative better food quality (Nishibe et al., 2010). Our results showed that the highest abundance of copepods found in the northern OS area, was associated with the lower abundance of microheterotrophs, and that the cyclopoid copepod, *Oithona atlantica*, was by far the most abundant species. Oithonids feed selectively on microzooplanktonic protists, such as ciliates and heterotrophic dinoflagellates (Nishibe et al., 2010; Zamora-Terol et al., 2013), and can therefore exploit microbial food webs more efficiently than calanoid copepods (Nielsen and Sabatini, 1996). The abundance of calanoid copepods was much lower than that previously recorded in this area during late spring and early summer, indicating an initial state in the seasonal succession of the mesozooplankton community (Ramirez, 1981, 2007). Therefore, we suggest that microzooplankton directly consumed much of the early spring phytoplankton production in the OS area, and processes that regulate this trophic linkage have major implications on the food web structure and secondary production of this ecosystem.

4.2. Shelf-break front

The main component of the bloom was identified as the small-sized (8.5–12.0 μm) diatom *Thalassiosira bioculata* var. *raripora* (Ferrario et al., 2013) reaching cell concentrations up to 4.5×10^3 - cells mL^{-1} associated to more than 90% of the total Chl *a* biomass (up to 20 mg m^{-3}). Several species of *Pseudo-nitzschia* and *Chaetoceros* (Ferrario, 2008; Sabatini et al., 2012) were secondary components (Diatoms PT-II). The dominance of *Pseudo-nitzschia* spp. and nanoplankton-sized diatoms from the genera *Thalassiosira* (<20 mμ) and *Chaetoceros* (<10 mμ), seemed to be a common feature of the spring bloom at the SBF (García et al., 2008; Gonçalves-Araujo et al., 2012; Ferreira et al., 2013).

T. bioculata var. *raripora* is common in large areas in the Norwegian Sea (Paasche and Rom, 1962), but has only occasionally been recorded in bloom concentrations (Paasche, 1961; Dale et al., 1999). In their study on the seasonal phytoplankton cycle at the high latitude (66°N, 2°E) oceanic site, M (Norwegian Sea), Dale et al. (1999) showed that, during the spring bloom in 1990 and 1992, *Fragilariopsis pseudonana* represented 98% and 95% of the diatoms, respectively. In 1991, however, *T. bioculata* var. *raripora* comprised 97% of the diatoms (0.45×10^3 cells mL^{-1}). According to Dale et al.,(1999), the variability in the abundance and species diversity of the phytoplankton community during the spring bloom appear to be determined by the species seeded during the pre-bloom period. To our knowledge, a resting stage remains

unknown for *T. bioculata* var. *raripora*, and its frustules have not been preserved in the diatom community from core top sediments collected in the SW Atlantic (Romero and Hensen, 2002). Spring bloom diatoms often form resting spores and resting cells in response to macronutrient and iron limitation as well as to the decline in light intensity (McQuoid and Hobson, 1996; Sugie et al., 2010). Our results showed that in the highly stratified northern region of the PSBF, a large fraction of the diatom bloom population (up to 85% at St11) was light-limited because they were confined below the MLD (26 ± 4 m). While sinking to greater depths, diatoms could form seed banks mostly dominated by "resting stages", as part of a long-term survival strategy, since they may constitute the next growth seasons seed population (Eilertsen et al., 1995; McQuoid et al., 2002; Rynearson et al., 2013). It is worth noting that the resting stage of diatom cells requires light to germinate during the pre-bloom period (Zhang and Lu, 2010). Therefore, the occurrence of upwelling along the PSBF, especially during late winter (Matano and Palma, 2008; Matano et al., 2010; Miller et al., 2011; Combes and Matano, 2014), could play an important role in helping the resting stages distributed in the deep layer, to be brought back to the euphotic layer and act as seeds for the next spring bloom. This has also been suggested for the upwelling systems of southern Benguela (Pitcher, 1990), British Columbia, Canada (Takahashi et al., 1977), and Kumano-Nada, Japan (Ishikawa et al., 2011). Despite the presence of sufficient seed population for a bloom in the water column, blooms cannot occur without the favorable environmental conditions required for rapid vegetative cell growth and cell accumulation. For instance, the rapid germination and high growth rates achieved by the spore-forming genus *Chaetoceros* (1 doubling day^{-1}) immediately after germination, seems to be the cause of the predominance of this genus in blooms at the mid and high latitudes (Rynearson et al., 2013). The timing of the spring bloom has traditionally been associated with the shoaling of the ML at the end of winter (Sverdrup, 1953). According to the critical depth hypothesis (Sverdrup, 1953), the spring bloom begins when the ML shoals become shallower than a Zcr, where the vertically integrated production in the mixed water column equals the vertically integrated losses. However, the value of the Zcr is subject to large uncertainties, partly due to the large interspecific variability of phytoplankton in the light-limiting threshold for cell growth (Falkowsky and Owens, 1980). Based on a review of available observations, it appears that the cell size can account for much of such interspecific variability (Edwards et al., 2015; Geider et al., 1986; Marañon, 2015). Small cell-sized diatoms (such as *T. bioculata* var. *raripora*) under nutrient-sufficient conditions, showed compensation depths with light intensities as low as 1 μmol quanta PAR m^{-2} s^{-1} (Falkowsky and Owens, 1980) and therefore a competitive advantage at light-limiting growth conditions. Unfortunately, our time of sampling prevented the measurement of the conditions prevailing at the initial stage of the bloom, even in the more bloom-delayed southern region (44–47°S). However, this southern region showed high Chl *a* concentrations (up to 779 mg m^{-2}), high macronutrient concentrations, low phytoplankton grazers and low stratification (the MLD averaged 60 m and ranged up to 97 m). The ML was deeper than both the euphotic zone and the calculated critical depth, and consequently, the average mixed layer PAR irradiance ($Ed_{[ML]}$) was low, especially at the core of the bloom (St35 = 1.46 and St42 = 2.04 mol quanta PAR m^{-2} d^{-1}). Therefore, it is reasonable to assume that during the initial stage (about two weeks before our observations), the diatom bloom occurred without or with an incipient vertical stratification. The observed high phytoplankton biomass with only minimal stratification (Townsend et al., 1992; Dale et al., 1999) is consistent with the hypothesis of critical turbulence (Huisman et al., 1999; Taylor and Ferrari, 2011a; Fischer et al., 2014). This hypothesis suggests that the spring bloom is triggered by a positive change in air-sea heat fluxes at the end of winter. This leads to the weakening of the turbulence in the mixed layer near the surface, allowing for the net growth of phytoplankton, while the response of the physical environment is slower than the biological response, and stratification just begins to develop.

Matano and Palma (2008) argued that the interaction of MC and bottom topography produces a cross-shelf divergence of the MC transport that leads to shelf-break upwelling, with the intensity proportional to the transport of the MC. Our *in situ* results showed that the intrusion of MCW onto the shelf (S_{III}) was accompanied by the upward displacement of high salinity, low temperature, macronutrient-rich waters, and therefore support this hypothesis. Therefore, the shelf-break upwelling region is a large source of macronutrients, especially nitrate (Carreto et al., 1995; García et al., 2008; Signorini et al., 2009) and probably dissolved iron (DFe), predominantly Fe(III) bound by organic Fe-complexing moieties, needed to sustain intense diatom blooms (Nakayama et al., 2010), such as those observed at the SBF during the austral spring. Although DFe concentrations were not measured during this cruise, we suspect that the interaction of the MC with the bottom topography near the shelf-break (Matano and Palma, 2008; Piola et al., 2010), and the consequent resuspension of Fe-rich sediments (originated in previous blooms) associated with advective upwelling, can be the principal source of DFe for the diatom bloom. Such sedimentary iron inputs associated with shallow topography are common features of phytoplankton blooms in the high-nutrient low-chlorophyll (HNLC) Southern Ocean (Klunder et al., 2011; Lai et al., 2008; Wadley et al., 2014), and in other HNLC regions downstream of continental shelves (Lam and Bishop, 2008). It is unlikely that the inner MC jet entrained DFe from near the shelf-break east of the Malvinas Islands (Signorini et al., 2009; Wadley et al., 2014), a region previously identified as having relatively high (4.4 nM) DFe concentrations (Bowie et al., 2002).

In this nutrient-rich and turbulent scenario, the initiation of phytoplankton growth could be more limited by light exposure than by the availability of nutrients. Frontal instabilities, however, can reduce the turbulent flux of phytoplankton cells out of the euphotic zone, thereby increasing the mean light exposure, and triggering the spring phytoplankton bloom (Taylor and Ferrari, 2011b). The MC shows a high heterogeneity, being formed by two main jets flowing along the 200 and 1400 m isobaths, which merge near 42°S to form a single jet farther north, and a series of secondary and discontinuous and highly intermittent high-velocity cores (Piola et al., 2013). Combes and Matano (2014) showed that in addition to the variability in the transport of the inshore portion of the MC, the impact of realistic bathymetry (e.g., canyons, changes of bottom slope, etc.) can lead to substantial modifications of the upwelling configuration, producing a strong upwelling and downwelling of cells along the PSBF. Our *in situ* observations south of 42°S also showed strong discontinuities in the MLD between the OS and the slope, but also between adjacent MC oceanic stations. On this basis, we suggest that the spring bloom in the SBF is elevated in phytoplankton biomass, due to intermittent periods of growth under reduced mixing near the surface (Huisman et al., 1999; Taylor and Ferrari, 2011a; Fischer et al., 2014; Daniels et al., 2015; Llort et al., 2015). This situation is punctuated by periods of more intense turbulence that redistribute the surface biomass to deeper and more nutrient-rich waters, where a diatom assemblage adapted to grow under low mean irradiance levels, replenishes the limiting nutrient and maintains growth and positive buoyancy (Geider et al., 1986; Acuña et al., 2010; Edwards et al., 2015). Thus, this mechanism is analogous to the nutrient-gathering migrations that some dinoflagellates undertake (Smayda and Trainer, 2010).

After this intermittent period, due to the accumulative effect of the surface heat flux in the air-sea interface, enhanced by the phytoplankton itself through light absorption (Frouin and

Iacobellis, 2002), the ML becomes shallower than the Zcr, as observed north of 42°S. As the blooms tend to begin in the north and develop progressively in the southward direction (Rivas et al., 2006; Carreto et al., 2007), the observed highly stratified northern region of the SBF (MLD 26 ± 4 m) likely reflects a late phase of the diatom bloom development. During the period of coccolithophore abundance (late spring), MLDs were typically <25 m north of 50°S (Painter et al., 2010). Painter et al. (2010) also observed small upward displacements of shallow isopycnal and isothermal surfaces in the vicinity of the SBF, suggesting the occurrence of weak localised upwelling.

In the northernmost section, the highest Chl *a* biomass (1162 mg m^{-2}) found at the shelf-break (St7) was partitioned above (605 mg m^{-2}) and below (557 mg m^{-2}) a shallow MLD (33 m). The euphotic depth (Ze = 11 m) is shallower than the MLD, and therefore the average mean mixed layer PAR was low ($Ed_{[ML]}$ = 3.4 mol quanta PAR m^{-2} d^{-1}). A direct consequence of the development of a strong, shallow stratification is that a significant diatom population was isolated below the MLD in an aphotic layer. For instance, a high diatom biomass (Chl *a* = 797 mg m^{-2}) representing up to 85% of total Chl *a*, was isolated in the aphotic zone below the shallow MLD (22 m) of St11 (S_{II}). During sinking, these light-limited diatoms can reach the shelf bottom directly, favouring the development of dense populations of the commercially important Patagonian scallop and the associated community (Mauna et al., 2011), as well as the formation of diatom seed banks and iron-rich sediments. At the deeper stations, diatom sedimentation can contribute to the biological pump by rapidly sinking to the ocean floor as relatively intact and sometimes viable cells (Salter et al., 2012; Rynearson et al., 2013; Onodera et al., 2015).

In the southernmost region the delayed diatom bloom was associated with high nitrate (9–10 μM) and phosphate (0.5–0.6 μM), but low silicic acid concentrations (~2.0 μM); the low Si:N ratio from 0.14 to 0.22, suggests a diatom bloom under progressive silicate limitation. However, the requirements of silica in diatom species can vary substantially (up to 4-fold) depending on cell size and frustule thickness. Small diatoms, such as *T. bioculata* var. *raripora*, do not appear to be subject to silicate or iron limitation to the same degree as larger diatoms (Martin-Jézéquel et al., 2000; Poulton et al., 2013). Moreover, under limiting silicate conditions diatoms can maintain near-maximum division rates, as their uptake is diminished to a greater extent than growth, leading to less silica being deposited during the cell cycle (Paasche, 1973; Brzezinsky et al., 1990). The observed higher silicic acid availability in the ML below the euphotic zone (~4 μM), where the diatom biomass was high, could favour their assimilation at depth. Although light availability is extremely low at this depth (<1%), mixing within the ML was probably sufficient to transport cells from the depths to the lighter layer, where the accumulation of carbohydrates is enhanced by higher photon flux densities. Because the energy for silicon metabolism is more closely linked to respiration than photosynthesis, silicic acid uptake and deposition can also occur in the light-limited and silicic acid-rich ML (Martin-Jézéquel et al., 2000;Claquin et al., 2002;Brown et al., 2003).

In contrast, in the highly stratified northern region of the SBF, phytoplankton nutrient consumption and development of a shallow ML, that prevents a steady nutrient input from below, cause very low nutrient concentrations and potentially limiting for the maintenance of diatom growth (1–2 μM nitrate, 0.3–0.4 μM phosphate, and 1–2 μM silicate). The low silicate concentrations and the relatively high Si:N ratios observed (up to 1.27) confirms that under limiting silicate conditions, the uptake of this nutrient is diminished to a greater extent than the others macronutrients, while diatom growth still continues (Brown et al., 2003). On the other hand, silicate regeneration in the upper mixed layer, via dissolution of biogenic silica, is also a critical silicate supply mechanism for diatoms (Bidle and Azam, 2001). In their review of silicon metabolism in diatoms, Martin-Jézéquel et al. (2000) compiled data for the Michaelis-Menten half-saturation constant for Si-dependent growth rates; the median half-saturation constant in 17 studies was 1.0 μM, leading to the assumption that the photosynthetic physiology of the diatom population in the present study was limited by Si. Nevertheless, the highest daily water-integrated primary production measured during this cruise (5.48 g C m^{-2} d^{-1}) was observed in this stratified area (Lutz et al., 2010). Chlorophyllide *a* and Chl *a* allomers have often been used as markers for senescent diatoms at the end of diatom blooms in coastal, open-ocean, and high-latitude environments (Jeffrey and Hallegraeff, 1987; Walker and Keely, 2004; Franklin et al., 2012; Bale et al., 2015). The relatively low concentrations of these pigments (chlorophyllide *a* = 1–3% of total Chl *a*) observed within the core of the bloom, suggest that the diatom population was not senescent. Satellite images documented that a week after our cruise, the bloom declination was well marked along the SBF. We suspect that bloom declination was associated with silicate limitation inducing diatom sedimentation and phytoplankton succession (Garcia et al., 2011; Poulton et al., 2013; Balch et al., 2014), as well as due to the losses produced by microzooplankton grazing, a process already initiated during the cruise in the western border of the shelf-break diatom bloom.

4.3. Malvinas current

The eastern core side of the MC despite its high macronutrient loading has been generally characterized as a permanently low chlorophyll region (HNLC) (García et al., 2008; Signorini et al., 2009; Painter et al., 2010; Poulton et al., 2013). Nevertheless, our results showed that even in the more oceanic MCW, the Chl *a* concentrations were typically >2.0 mg m^{-3}, north of 42°S, and <2.0 mg m^{-3}, south of this latitude. Therefore, the oceanic MC ecosystem can be considered as two latitudinal regions; the highly stratified high-chlorophyll north of 42°S, and the less stratified high-nutrient low-chlorophyll (HNLC) south of 42°S. As in the SBF, the more northern station (St8) of the MC showed a remarkable bloom (Chl *a* up to 6.4 mg m^{-3}) of *T. bioculata* var. *raripora* (Diatoms TP-1 = 67–72% and Diatoms TP-2 = 19–30% of total Chl *a*), whereas the contribution of haptophytes, the second abundant group, was small (1–5%). A large fraction of the diatom bloom was below a shallow MLD (24 m), and the average mean mixed layer PAR was relatively low ($Ed_{[ML]}$= 7 mol quanta PAR m^{-2} d^{-1}). Nutrients at the surface waters showed high nitrate (~6 μM) and phosphate (~0.5 μM) but very low silicic acid concentrations (<1.0 μM), and the diatom population was probably under silicate limitation. However, the high daily rates of water-integrated primary production (Lutz et al., 2010) and the low concentration of chlorophyllide *a* (1–3% of total Chl *a*) and Chl *a* allomers (traces) confirmed that the diatom population was not senescent (Franklin et al., 2012; Walker and Keely, 2004; Bale et al., 2015). Moreover, the paucity of microzooplankton and the absence of degraded fucoxanthin pigments suggest that losses due to microzooplankton grazing were low. A scenario showing a diatom bloom associated with silica depletion indicated the existence of a source of DFe (Brzezinski et al., 2001, 2005) fertilizing this northern area. Bowie et al. (2002) made a few measurements of DFe in the region, and reported a maximum of 1.7 nM in the front of the sub-tropical convergence zone, towards Uruguay at 35°S. Recently, Rijkenberg et al. (2014) reported that the higher DFe concentrations (up to 6.1 nM) of the southwest Atlantic were found at the BMC (35–40°S). Due to the fact that the high DFe concentrations were not associated with a minimum in salinity, Rijkenberg et al. (2014) suggest that these high DFe concentrations were not part of the Rio de la Plata plume; instead, the enrichment was due to the offshore export of Brazilian shelf waters (Attisano et al., 2013) near the BMC (see Matano et al.,

2014). Complementary to the *in situ* growth hypothesis, the high diatom biomass observed in the northernmost station (St8) may be also due to their transport from the adjacent shelf-break bloom station, as occurring near the BMC (Matano et al., 2010, 2014; Guerrero et al., 2014; Strub et al., 2015). The off-shelf transport of high chlorophyll waters near the BMC (captured in chlorophyll images) represents a significant loss of phytoplankton biomass that does not reach the sediments of the continental slope.

The HNLC region showed a high-diversity low-phytoplankton biomass community (Chl $a = 0.4$ to $0.8\ mg\ m^{-3}$) dominated by small cells, in which the contribution of diatoms to total Chl *a*, was relatively high (30–60%). Diatoms PT2a group probably related to the small diatoms (<5 μm) observed by Ferrario (2008), were the more important component of this phytoplankton assemblage. Haptophytes, chlorophytes, prasinophytes, and cryptophytes were also relevant, while the contribution of dinoflagellates and cyanobacteria were very small. Among haptophytes, *Phaeocystis*-PT8 (7–14%) (García et al., 2008) and *Chrysochromulina*-PT7 (2–15%) were the more important members of this phytoplankton assemblage, whereas the contribution of the *Emiliania*-PT6 group to total Chl *a* was relatively low (1–5%). Indications of phytoplankton growth limitation in the HNLC region can be inferred from ocean color images, showing the annual persistency of low Chl *a* concentrations (Saraceno et al., 2005; Rivas et al., 2006; Romero et al., 2006). Although previous studies provided evidence that Patagonian dust plumes and volcanic ash may play a significant role in the iron fertilization of the South Atlantic Ocean (see review of Signorini et al., 2009), recent studies (Johnson et al., 2011) suggest that they are not likely to be the major source of bioavailable iron. Moreover, low DFe concentrations (~0.2 nM) were observed far from the continental margin (Bowie et al., 2002; Rijkenberg et al., 2014). Therefore, as in other HNLC regions, iron appeared to be the potential limiting factor for phytoplankton growth. However, oceanic and neritic phytoplankton species can be distinguished from each other by their tolerance to low iron concentrations. For instance, unlike many other *Thalassiosira* species that were predominantly found in coastal waters, *Thalassiosira oceanica* is adapted to oligotrophic conditions and is highly tolerant to iron-limitation in particular (Lommer et al., 2012). Our results showed the characteristic low Si:N ratios of Subantarctic waters (~0.45), but silicic acid concentrations within the euphotic zone were much higher (~7 μM) than those observed in the northern region (<1 μM), indicating that other factors, like DFe, were potentially limiting diatom growth. Results of the Southern Ocean Iron Experiment (SOFeX) support this idea, showing that iron increased the ability of Subantarctic diatom assemblages to take up low concentrations of silicate, over an order of magnitude, by increasing maximum uptake rates and lowering half-saturation constants for silicic acid uptake (Brzezinski et al., 2005). Nevertheless, the low silicic acid concentrations (~1 μM) observed in late spring (Painter et al., 2010) indicates that during the spring, the diatom population consumed most of the silicic acid available. Therefore, although phytoplankton growth rates could be principally limited by iron, other losses such as strong grazing pressure and/or cell advection could be important. It has been noted (García et al., 2008) that the transport dynamics of the high-velocity MC jet can produce significant losses of phytoplankton cells by advection when cell division rates are low.

5. Conclusions

- A remarkable *quasi* monospecific bloom (~90%) of a nanodiatom (*Thalassiosira bioculata* var. *raripora*) associated with high Chl *a* (up to $20\ mg\ m^{-3}$) occurred in spring along (~1000 km) the Patagonian shelf-break front.
- The bloom was located along the front formed at the meeting of SASW and MCW. The interaction of the MC with the bottom topography near the shelf-break and the associated upwelling provides a large source of macronutrients and probably the DFe needed to sustain large diatom blooms during spring.
- The bloom initiation occurred with minimal stratification, probably triggered by a positive change in air-sea heat fluxes at the end of winter, leading to a weakening of the turbulence in the mixed layer near the surface. These events appeared to be punctuated by periods of more intense turbulence related to the MC dynamic.
- Following the north-south progression in solar radiation and day length, there was a latitudinal delay in bloom development and phytoplankton succession, with the northern part showing a late development stage, while the southern part representing an earlier development stage.
- A strong shallow stratification developed during the late phase of the bloom, inducing the sinking of the diatom population isolated below the MLD, thereby favouring the development of epibenthic communities, the formation of seed diatom banks, and the return of organic iron to the sediments. At the deeper stations, diatom sedimentation can contribute to the biological pump by rapidly sinking at the ocean floor.
- During the late phase of the bloom, silicic acid limitation appeared to be an importantfactor controlling the spring bloom decay and phytoplankton succession.
- Losses due to microzooplankton grazing pressure –mainly heterotrophic dinoflagellates of the genus *Protoperidinium*–estimated by the presence of high amounts of a fucoxanthin derivative (F459), appear to be another important factor controlling the spring bloom decay and the structure of the plankton community in the western border of the shelf-break diatom bloom. Feeding of microheterotrophs by an oithonid copepod also suggests a further temporal step in the plankton succession in this area.

Acknowledgements

This work was facilitated by the contribution of many colleagues who provided us instruments, help on board, unpublished data, but mostly useful advices. Among them we wish to thank: A. Bianchi, A. Callone, E. Cozzolino, V. Lutz and A. Piola. We are also grateful to M.D. Makey for providing the computer program CHEMTAX. We are thankful for the constructive criticism of two anonymous reviewers, which greatly improved the manuscript. This work was financed by INIDEP and grants from: "Fundación Antorchas" (Grant 13900-13), PNUDARG02/018) (BB23 and BB33), CONICET PIP-112-201101-00892, and the Inter-American Institute for Global Change Research (IAI) CRN 3070 sponsored by the US National Science Foundation Grant GEO-0452325. This is INIDEP contribution N° 1983.

Appendix A. Supplementary material

Supplementary data associated with this article can be found, in the online version, at http://dx.doi.org/10.1016/j.pocean.2016.05.002.

References

Acha, E.M., Mianzan, H., Guerrero, R., Favero, M., Bava, J., 2004. Marine fronts at the continental shelves of austral South America. Physical and ecological processes. Journal of Marine Systems 44, 83–105.

Acha, E.M., Iribarne, O., Piola, A., Mianzan, H., 2015. Ecological processes at marine fronts. Oases in The Ocean. Springer Briefs in Environmental Science. Springer, Swizerland, 77 pp..

Acuña, J.L., López-Alvarez, M., Nogeira, E., González-Taboada, F., 2010. Diatom flotation at the onset of the spring phytoplankton bloom: an in situ experiment. Marine Ecology Progress Series 400, 115–125. http://dx.doi.org/10.3354/meps08405.

Alemany, D., Acha, M.E., Iribarne, O., 2009. The relationship between marine fronts and fish diversity in the Patagonian Shelf Large Marine Ecosystem. Journal of Biogeography 36, 2111–2124.

Alemany, D., Acha, M.E., Iribarne, O., 2014. Marine fronts are important fishing areas for demersal species at the Argentine Sea (South West Atlantic Ocean). Journal of Sea Research 87, 56–67.

Akselman, R., Negri, R.M., Cozzolino, E., 2014. Azadinium (Amphidomataceae, Dinophyceae) in the Southwest Atlantic: in situ and satellite observations. Revista de Biología Marina y Oceanografía 49, 511–526.

Akselman, R., Negri, R.M., 2012. Blooms of Azadinium cf. spinosum Elbrächter et Tillmann (Dinophyceae) in northern shelf waters of Argentina, Southwestern Atlantic. Harmful Algae 19, 30–38.

Attisano, K.K., Rodrigues Santos, I., Ferreira de Andrade, C.F., Lopes de Paiva, M., Bigliardi Milani, I.C., Niencheski, L.F.H., 2013. Submarine groundwater discharge revealed by radium isotopes (ra-223 and ra-224) near a paleochannel on the southern Brazilian continental shelf. Brazilian Journal of Oceanography 61 (3), 195–200.

Balch, W.M., Drapeau, D.T., Bowler, B.C., Lyczkowski, E.R., Lubelczyk, L.C., Painter, S. C., Poulton, A.J., 2014. Surface biological, chemical, and optical properties of the Patagonian Shelf coccolithophore bloom, the brightest waters of the Great Calcite Belt. Limnology and Oceanography 59 (5), 1715–1732. http://dx.doi.org/10.4319/lo.2014.59.5.1715.

Bale, N.J., Airs, R.L., Martin, P., Lampitt, R.S., Llewelling, C.A., 2015. Chlorophyll-a transformations associated with sinking diatoms during termination of a North Atlantic spring bloom. Marine Chemistry 172, 23–33.

Berastegui, A.D., Menu Marques, S., Gómez-Erache, M., Ramirez, F.C., Mianzan, H.W., Acha, E.M., 2006. Copepod assemblages in a highly complex hydrographic region. Estuarine, Coastal and Shelf Science 66, 483–492.

Bertolotti, M.I., Brunetti, N.E., Carreto, J.I., Prenski, L.B., Sánchez, R.P., 1996. Influence of shelf-break fronts on shellfish and fish stocks off Argentina, CM1996/S: 41, International Council for the Exploration of the Sea, Cophenhagen, Denmark 15pp.

Bianchi, A.A., Pino, D.R., Perlender, H.G.I., Osiroff, A.P., Segura, V., Lutz, V., Clara, M.L., Balestrini, C.F., Piola, A.R., 2009. Annual balance and seasonal variability of sea–air CO_2 fluxes in the Patagonia Sea: their relationship with fronts and chlorophyll distribution. Journal of Geophysical Research 114, C03018. http://dx.doi.org/10.1029/2008JC004854.

Bidle, K.D., Azam, F., 2001. Bacterial control of silicon regeneration from diatom detritus: significance of bacterial ectohydrolases and species identity. Limnology and Oceanography 46 (7), 1606–1623.

Boltovskoy, D., 1981. Atlas del zooplancton de Atlántico Sudoccidental y métodos de trabajo con el zooplancton marino. Instituto Nacional de Investigación y Desarrollo Pesquero, INIDEP. Mar del Plata, Argentina, pp. 936.

Bowie, A.R., Whitworth, D.J., Achterberg, E.P., Fauzi, R., Mantoura, C., Worsfold, P.J., 2002. Biogeochemistry of Fe and other trace elements (Al, Co, Ni) in the upper Atlantic Ocean. Deep Sea Research Part I 49, 605–636.

Brown, L., Sanders, R., Deacon, G., Savidge, G., Lucas, C.H., 2003. The uptake of silica during the spring bloom in the Northeast Atlantic Ocean. Limnology and Oceanography 48 (5), 1831–1845.

Brzezinski, M.A., Olson, R.J., Chisholm, S.W., 1990. Silicon availability and cell-cycle progression in marine diatoms. Marine Ecology Progress Series 67, 83–96.

Brzezinski, M.A., Jones, J.L., Demarest, M., 2005. Control of silica production by iron and silicic acid during the Southern Ocean Iron Experiment (SOFeX). Limnology and Oceanography 50 (3), 810–824.

Brzezinski, M.A., Nelson, D.M., Franck, V.M., Sigmon, D.E., 2001. Silicon dynamics within an intense open-ocean diatom bloom in the Pacific sector of the Southern Ocean. Deep Sea Research Part II—Topical Studies in Oceanography 48, 3997–4018.

Buskey, E.J., Coulter, C.J., Brown, S.L., 1994. Feeding, growth and bioluminescence of the heterotrophic dinoflagellate *Protoperidinium huberi*. Marine Biology 121, 373–380.

Calbet, A., Landry, M.R., 2004. Phytoplankton growth, microzooplankton grazing and carbon cycling in marine systems. Limnology and Oceanography 49 (1), 51–57.

Carreto, J.I., 1985. A new ketocarotenoid from the heterotrophic dinoflagellate *Protoperidinium depressum* (Bayley) Balech. Journal of Plankton Research 7 (3), 421–423.

Carreto, J.I., Benavides, H.R., Negri, R.M., Glorioso, P.D., 1986. Toxic red-tide in the Argentine Sea. Phytoplankton distribution and the survival of the toxic dinoflagellate *Gonyaulax excavata* in a frontal area. Journal of Plankton Research 8 (1), 15–28.

Carreto, J.I., Montoya, N.G., Benavides, H.R., Guerrero, R., Carignan, M.O., 2003. Characterisation of spring phytoplankton communities in the Río de la Plata maritime front and the adjacent subtropical confluence area using pigment signatures and cell microscopy. Marine Biology 143, 1013–1027.

Carreto, J.I., Lutz, V.A., Carignan, M.O., Cucchi Colleoni, A.D., De Marco, S.G., 1995. Hydrography and chlorophyll *a* in a transect from the coast to the shelf-break in the Argentinian Sea. Continental Shelf Research 15, 315–336.

Carreto, J.I., Carignan, M.O., Montoya, N.G., Cucchi Colleoni, D.A., 2007. Ecología del fitoplancton en los sistemas frontales del Mar Argentino. In: Carreto, J.I., Bremec, C. (Eds.), El Mar Argentino y sus recursos Pesqueros V: El ambiente Marino, INIDEP, Mar del Plata (Argentina), pp. 11–31.

Carreto, J.I., Montoya, N.G., Akselman, R., Carignan, M.O., Silva, R.I., Cucchi Colleoni, D.A., 2008. Algal pigment patterns and phytoplankton assemblages in different water masses of the Río de la Plata maritime front. Continental Shelf Research 28, 1589–1607.

Claquin, P., Martin-Jézéquel, V., Kromkamp, J.C., Veldhuis, M.J., Kraay, G.W., 2002. Uncoupling of silicon compared with carbon and nitrogen metabolisms and the role of the cell cycle in continuous cultures of *Thalassiosira pseudonana* (Bacillariophyceae), under light, nitrogen and phosphorus control. Journal of Phycology 38, 922–930.

Charo, M., Piola, A., 2014. Hydrographic data from the GEF Patagonia cruises. Earth System Science Data 6, 265–271. http://dx.doi.org/10.5194/essd-6-265.

Chen, N., Bianchi, T.S., Bland, J.M., 2002. Novel decomposition products of chlorophyll-*a* in continental shelf (Louisiana Shelf) sediments: formation and transformation of carotenol chlorin esters. Geochimica et Cosmochimica Acta 67 (11), 2027–2042.

Combes, V., Matano, R.P., 2014. A two-way nested simulation of the oceanic circulation in the Southwestern Atlantic. Journal of Geophysical Research: Oceans 119, 731–756. http://dx.doi.org/10.1002/2013JC009498.

Dale, T., Rey, F., Heimdal, B., 1999. Seasonal development of phytoplankton at a high latitude oceanic site. Sarsia 85, 419–435.

Daniels, C.J., Poulton, A.J., Esposito, M., Paulsen, M.L., Bellerby, R., St. John, M., Martin, A.P., 2015. Phytoplankton dynamics in contrasting early stage North Atlantic spring blooms: composition, succession, and potential drivers. Biogeosciences Discussions 12, 93–133.

De Boyer Montégut, C., Madee, G., Fisher, A.S., Lazer, A., Ludicone, D., 2004. Mixed layer depth over the global ocean: an examination of profile data and a profile based climatology. Journal of Geophysical Research 109, c12003. http://dx.doi.org/10.1029/2004JC002378.

De Souza, M.S., Borges Mendes, C.F., García, V.M.T., Pollery, R., Brodas, V., 2012. Phytoplankton community during a coccolithophorid bloom in the Patagonian shelf: microscopic and high-performance liquid chromatography pigments analyses. Journal of the Marine Biological Association of the United Kingdom 92 (1), 13–27. http://dx.doi.org/10.1017/SA0025315411000439.

Edwards, K.F., Thomas, M.K., Christopher, A., Klausmeier, C.A., Litchman, E., 2015. Light and growth in marine phytoplankton: allometric, taxonomic, and environmental variation. Limnology and Oceanography 60 (2), 540–552.

Eilertsen, H., Sandberg, S., Tøllefsen, H., 1995. Photoperiodic control of diatom spore growth: a theory to explain the onset of phytoplankton blooms. Marine Ecology Progress Series 116, 303–307.

Falkowsky, P.G., Owens, T.G., 1980. Light-shade adaptation: two strategies in marine phytoplankton. Plant Physiology 66, 592–595.

Ferrario, M.E., Almandoz, G.O., Cefarelli, A.O., Sastre, V., Santinelli, N., 2013. Ultrastructure of Thalassiosira bioculata var. rariprora in the Argentine Sea slope. First record for the Southern Hemisphere. X International Phycological Congress. Orlando, USA.

Ferrario, M.E., 2008. Biodiversidad y dinámica estacional del fitoplankton en la Patagonia: el área del talud y de la plataforma adyacente. Proyecto GEF Patagonia (Argentina). Informe Subproyecto BB33, 43 pp. <www.ambiente.gov.ar/archivos/web/GTRA/file/.../plancton/BB33.pdf>.

Ferreira, A., Stramski, D., Garcia, C.A.E., Garcia, V.M.T., Ciotti, A.M., Mendes, C.R.B., 2013. Variability in light absorption and scattering of phytoplankton in Patagonian waters: Role of community size structure and pigment composition. Journal of Geophysical Research: Oceans 118, 698–714. http://dx.doi.org/10.1002/jgrc.20082.

Fischer, A.D., Moberg, E.A., Alexander, H., Brownlee, E.F., Hunter-Cevera, K.R., Pitz, K. J., Rosengard, S.Z., Sosik, H.M., 2014. Sixty years of Sverdrup: a retrospective of progress in the study of phytoplankton blooms. Oceanography 27 (1), 222–235.

Franklin, D.J., Airs, R.L., Fernandes, M., Thomas, G., Bell, T.G., Bongaerts, R.J., Berges, J. A., Malin, G., 2012. Identification of senescence and death in Emiliania huxleyi and Thalassiosira pseudonana: cell staining, chlorophyll alterations, and dimethylsulfoniopropionate (DMSP) metabolism. Limnology and Oceanography 57 (1), 305–317.

Frouin, R.J., Iacobellis, S.F.I., 2002. Influence of phytoplankton on the global radiation budget. Journal of Geophysical Research 107, 4377. http://dx.doi.org/10.1029/2001JD000562.

García, V.T.M., Garcia, C.A.E., Mata, M.M., Pollery, R.C., Piola, A.R., Signorini, S.R., McClain, C.R., Iglesias-Rodriguez, M.D., 2008. Environmental factors controlling the phytoplankton blooms at the Patagonia shelf-break in spring. Deep Sea Research Part I 55, 1150–1166.

Garcia, C.A.E., García, V.T.M., Dogliotti, A.I., Ferreira, A., Romero, S.I., Mannino, A., Souza, M.S., Mata, M.M., 2011. Environmental conditions and biooptical signature of a coccolithophorid bloom in the Patagonian shelf. Journal of Geophysical Research 111, C03025. http://dx.doi.org/10.1029/2010JC006595.

Garrido, J.I., Airs, R.L., Rodriguez, F., Van Heukelem, L., Zapata, M., 2011. New HPLC separation techniques. In: Roy, S., Llewellyn, C.A., Egeland, E.S., Johnsen, G. (Eds.), Phytoplankton Pigments: Characterization, Chemotaxonomy and Application in Oceanography. Cambridge University Press, New York, pp. 165–179.

Gayoso, A.M., 1995. Bloom of *Emiliania huxleyi* (Prymnesiophyceae) in the western South Atlantic Ocean. Journal of Plankton Research 17, 1717–1722.

Geider, R.J., Platt, T., Raven, J.A., 1986. Size dependence of growth and photosynthesis in diatoms: a synthesis. Marine Ecology Progress Series 30, 93–104.

Goericke, R., Shankle, A., Repeta, D.J., 1999. Novel carotenol chlorin in marine sediments and water column particulate matter. Geochimica et Cosmochimica Acta 63 (18), 2825–2834.

Goericke, R., Strom, S.L., Bell, M.A., 2000. Distribution and sources of cyclic pheophorbides in the marine environment. Limnology and Oceanography 45 (1), 200–211.

Gonçalves-Araujo, R., De Souza, M.S., Borges Mendes, C.R., Tavano, V.M., Pollery, R. C., Eiras Garcia, C.A.E., 2012. Brazil-Malvinas confluence: effects of environmental variability on phytoplankton community structure. Journal of Plankton Research 34 (5), 399–415. http://dx.doi.org/10.1093/plank/fbs013.

Grasshoff, K., Ehrhardt, M., Kremling, K., 1983. Methods of Seawater Analysis. Verlag Chemie, Weinheim, 419 pp..

Guerrero, R.A., Piola, A.R., 1997. Masas de agua en la Plataforma Continental. In: Boschi, E. (Ed.), El Mar Argentino y sus Recursos Pesqueros I: Antecedentes históricos de las exploraciones en el mar y las características ambientales. Instituto Nacional de investigación y Desarrollo Pesquero, Mar del Plata, Argentina, pp. 107–118.

Guerrero, R.A., Piola, A.R., Fenco, H., Matano, R.P., Combes, V., Charo, Y., James, C., Palma, E.D., Saraceno, M., Strub, P.T., 2014. The salinity signature of the cross-shelf exchanges in the southwestern Atlantic Ocean: satellite observations. Journal of Geophysical Research: Oceans 119. http://dx.doi.org/10.1002/2014JC010113.

Harradine, P.J., Harris, P.G., Heat, R.N., Harris, R.P., Maxwell, J.R., 1996. Steryl chlorin esters are formed by zooplankton herbivory. Geochimica et Cosmochimica Acta 60, 2265–2270.

Higgins, H.W., Wright, S.W., Schlüter, L., 2011. Quantitative interpretation of chemotaxonomic pigment data. In: Roy, S., Llewellyn, C.A., Egeland, E.S., Johnsen, G. (Eds.), Phytoplankton Pigments: Characterization, Chemotaxonomy and application in Oceanography. Cambridge University Press, New York, pp. 257–301.

Huisman, J., van Oostveen, P., Weissing, F.J., 1999. Critical depth and critical turbulence: two different mechanisms for the development of phytoplankton blooms. Limnology and Oceanography 4 (1), 781–787.

Ishikawa, A., Kitami, S., Ishii, K., Nakamura, T., Imai, I., 2011. Resting stage cells of diatoms in deep waters in Kumano-Nada, central part of Japan. Plankton and Benthos Research 6 (4), 206–209.

Jacobson, D.M., Anderson, D.M., 1986. Thecate heterotrophic dinoflagellates: feeding behavior and mechanisms. Journal of Phycology 22, 249–258.

Jeffrey, S.W., Hallegraeff, G.M., 1987. Chlorophyllase distribution in ten classes of phytoplankton: a problem for chlorophyll analysis. Marine Ecology Progress Series 35, 293–304.

Jeffrey, S.W., Wright, S.W., 1997. Qualitative and quantitative HPLC analysis of SCOR reference algal cultures. In: Jeffrey, S.W., Mantoura, R.F.C., Wright, S.W. (Eds.), Phytoplankton Pigments in Oceanography: Guidelines to Modern Methods, vol. 10. UNESCO Monographs on Oceanographic Methodology, Paris, pp. 343–360.

Jeffrey, S.W., Wright, S.W., Zapata, M., 2011. Microalgal classes and their signature pigments. In: Roy, S., Llewellyn, C.A., Egeland, E.S., Johnsen, G. (Eds.), Phytoplankton Pigments: Characterization, Chemotaxonomy and application in Oceanography. Cambridge University Press, New York, pp. 3–45.

Jeong, H.J., Yoo, Y.D., Kim, J.S., Kan, N.S., Kim, T.H., 2012. Growth, feeding and ecological roles of the mixotrophic and heterotrophic dinoflagellates in marine planktonic food webs. Ocean Science Journal 45 (2), 65–91. http://dx.doi.org/10.1007/s12601-010-0007-2.

Johnson, M.S., Meskhidze, N., Kiliyanpilakkil, V.P., Gassó, S., 2011. Understanding the transport of Patagonian dust and its influence on marine biological activity in the South Atlantic Ocean. Atmospheric Chemistry and Physics 11, 2487–2502.

Klunder, M.B., Laan, P., Middag, R., De Baar, H.J.W., van Ooijen, J.C., 2011. Dissolved iron in the Southern Ocean (Atlantic sector). Deep Sea Research II 58, 2678–2694. http://dx.doi.org/10.1016/j.dsr2.2010.10.042.

Kozlowki, W.A., Deutschman, D., Garibotti, D., Trees, Ch., Vernet, M., 2011. An evaluation of the application of CHEMTAX to Antarctic coastal pigment data. Deep Sea Research Part I 58, 350–364.

Lai, X., Norisuye, K., Mikata, M., Minami, T., Bowie, A.R., Sohrin, Y., 2008. Spatial and temporal distribution of Fe, Ni, Cu and Pb along 140°E in the Southern Ocean during summer 2001/02. Marine Chemistry 111, 171–183.

Lam, P.J., Bishop, J.K.B., 2008. The continental margin is a key source of iron to the HNLC North Pacific Ocean. Geophysical Research Letters 35, L07608. http://dx.doi.org/10.1029/2008GL033294.

Llewellyn, C.A., Gibb, S.W., 2000. Intra-class variability in the carbon, pigment and biomineral content of prymnesiophytes and diatoms. Marine Ecology Progress Series 193, 33–44.

Llort, J., Lévy, M., Sallée, J.-B., Tagliabue, A., 2015. Onset, intensification and decline of phytoplankton blooms in the Southern Ocean. ICES Journal of Marine Science. http://dx.doi.org/10.1093/icesjms/fsv053.

Löder, M.G., Meunier, C., Wiltshire, K.H., Boersma, M., Aberle, N., 2011. The role of ciliates, heterotrophic dinoflagellates and copepods in structuring spring plankton communities at Helgoland Roads, North Sea. Marine Biology 158, 1551–1580.

Lommer, M., Specht, M., Roy, A.S., Kraemer, L., Andreson, R., Gutowska, M.A., Wolf, J., Bergner, S.V., Schilhabel, M.B., Klostermeier, U.C., Beiko, R.G., Rosenstiel, P., Hippler, M., LaRoche, J., 2012. Genome and low-iron response of an oceanic diatom adapted to chronic iron limitation. Genome Biology 13, R66.

Louda, J.W., Mongkhonsri, P., Baker, E.W., 2011. Chlorophyll degradation during senescence and death-III: 3–10 yr experiments. Organic Geochemistry 42, 688–699.

Lutz, V.A., Segura, V., Dogliotti, A.I., Gagliardini, D.A., Bianchi, A.A., Balestrini, C.F., 2010. Primary production in the Argentine Sea during spring estimated by field and satellite models. Journal of Plankton Research 32 (2), 181–195. http://dx.doi.org/10.1093/plankt/fbp117.

Mackey, M.D., Mackey, D.J., Higgins, H.W., Wright, S.W., 1996. A program for estimating class abundances from chemical markers: application to HPLC measurements of phytoplankton. Marine Ecology Progress Series 144, 265–283. http://dx.doi.org/10.3354/meps144265.

Marañon, E., 2015. Cell size as a key determinant of phytoplankton metabolism and community structure. Annual Review of Marine Science 7, 241–264.

McQuoid, M.R., Hobson, L.A., 1996. Diatom resting stages. Journal of Phycology 32 (6), 889–902.

McQuoid, M.R., Godhe, A., Nordberg, K., 2002. Viability of phytoplankton resting stages in the sediments of a coastal Swedish fjord. European Journal of Phycology 37, 191–201.

Matano, R.P., Palma, E.D., 2008. On the upwelling of downwelling currents. Journal of Physical Oceanography 38 (11), 2482–2500.

Matano, R.P., Palma, D.E., Piola, A.R., 2010. The influence of the Brazil and Malvinas Currents on the Southwestern Atlantic Shelf circulation. Ocean Science 6, 983–995.

Matano, R.P., Combes, V., Piola, A.R., Guerrero, R., Palma, E.D., Strub, P.T., James, C.H., Fenco, C.H., Chao, Y., Saraceno, M., 2014. The salinity signature of the cross-shelf exchanges in the Southwestern Atlantic Ocean: numerical simulations. Journal of Geophysical Research: Oceans 119, 2014J. http://dx.doi.org/10.1002/C010116.

Martin-Jézéquel, V., Hildebrand, M., Brzezinsky, M.A., 2000. Silicon metabolism in diatoms: Implications for growth. Journal of Phycology 36, 821–840.

Mauna, A.C., Botto, F., Franco, B., Schwatz, J.M., Acha, M., Lasta, M., Iribarne, O., 2011. Shifts in a epibenthic trophic web across a marine frontal area in the Southwestern Atlantic (Argentina). Journal of Sea Research 66, 245–255.

Miller, R.N., Matano, R.P., Palma, E.D., 2011. Shelfbreak upwelling induced by alongshore currents: analytical and numerical results. Journal of Fluid Mechanics 686, 239–249.

Montagnes, D.J.S., Dower, J.F., Figueiredo, G.M., 2010. The protozooplankton-ichthyoplankton trophic link: an overlooked aspect of aquatic food webs. Journal of Eukaryotic Microbiology 57, 223–228.

Motoda, S., 1969. Devices of Simple Plankton Apparatus IV. Bulletin of the Faculty of Fisheries, Hokkaido University, vol. 20, pp. 183–187.

Nakayama, Y., Kuma, K., Fujita, S., Sugie, K., Ikeda, T., 2010. Temporal variability and bioavailability of iron and other nutrients during the spring phytoplankton bloom in the Oyashio región. Deep Sea Research Part II: Topical Studies in Oceanography 57 (17), 1618–1629.

Negri, R.M., Carreto, J.I., Benavides, H.R., Akselman, R., Lutz, V.A., 1992. An unusual bloom of *Gyrodinium* cf. *aureolum* in the Argentine Sea. Community structure and conditioning factors. Journal of Plankton Research 14 (2), 261–269.

Negri, R.N., Silva, R., Viñas, M.D., 2003. Distribución de Gephyrocapsa oceanica (Haptophyta) en un sector de la plataforma Argentina (Atlántico Sudoccidental, 27–40 S). Boletín de la Sociedad Argentina de Botánica 38, 131–137.

Nelson, D.M., Smith, W.O., 1991. Sverdrup revisited: critical depths, maximum chlorophyll Levels, and the control of Southern Ocean productivity by the irradiance-mixing regime. Limnology and Oceanography 36 (8), 1650–1661.

Neveux, J., Soyer, M.D., 1976. Characterization des pigments et structure fine de *Protoperidinium ovatum* Pouchet (Dinoflagellata). Vie Milieu Serie A 27, 175–199.

Nielsen, T.G., Sabatini, M., 1996. Role of the copepod *Oithona* spp. in North Sea plankton communities. Marine Ecology Progress Series 139, 79–93.

Nishibe, Y., Kobari, T., Ota, K., 2010. Feeding by the cyclopoid copepod *Oithona similis* on the microplankton assemblage in the Oyashio region during spring. Plankton and Benthos Research 5 (2), 74–78.

Onodera, J., Watanabe, E., Harada, N., Honda, M.C., 2015. Diatom flux reflects water-mass conditions on the southern Northwind Abyssal Plain, Arctic Ocean. Biogeosciences 12, 1373–1385.

Paasche, E., 1961. Notes on phytoplankton from the Norwegian Sea. Botanica Marina 2 (3/4), 197–214.

Paasche, E., Rom, A.M., 1962. On the phytoplankton vegetation of the Norwegian Sea in May 1958. Nytt Magasin for Botanik 9, 33–60.

Paasche, E., 1973. Silicon and the ecology of marine plankton diatoms. II. Silicate-uptake kinetics in five diatoms species. Marine Biology 19 (3), 262–269.

Painter, S.C., Poulton, A.J., Allen, J.T., Pidcock, R., Balch, W.M., 2010. The COPAS'08 expedition to the Patagonian Shelf: physical and environmental conditions during the 2008 coccolithophore bloom. Continental Shelf Research 30, 1907–1923.

Piola, A.R., Franco, B.C., Palma, E.D., Saraceno, M., 2013. Multiple jets in the Malvinas Current. Journal of Geophysical Research: Oceans 118, 2107–2117. http://dx.doi.org/10.1002/jgrc.20170.

Piola, A.R., Rivas, A.L., 1997. Corrientes en la plataforma continental. In: Boschi, E.E. (Ed.), El Mar Argentino y sus recursos pesqueros, I: Antecedentes históricos de las exploraciones en el Mar Argentino y las características ambientales. Instituto Nacional de investigación y Desarrollo Pesquero, Mar del Plata, Argentina, pp. 119–132.

Piola, A.R., Campos, E.J.D., Moéller, O.O., Charo, M., Martinez, C., 2000. Subtropical Shelf Front off eastern South America. Journal of Geophysical Research: Oceans 105, 6565–6578.

Piola, A.R., Martinez Avellaneda, N., Guerrero, R.A., Jardón, F.P., Palma, E.D., Romero, S., 2010. Malvinas slope water intrusions on the northern Patagonia continental shelf. Ocean Science 6, 345–359. http://dx.doi.org/10.5194/os-6-3452010, ISSN: 1812-0784.

Pitcher, G.C., 1990. Phytoplankton seed populations of the Cape Peninsula upwelling plume, with particular reference to resting spores of *Chaetoceros* (Bacillariophyceae) and their role in seeding upwelling waters. Estuarine, Coastal and Shelf Science 31, 283–301.

Podestá, G.P., 1988. Migratory pattern of Argentina hake (*Merluccius hubbsi*) and oceanic processes in the Southwestern Atlantic Ocean. Fishery Bulletin 88, 167–177.

Poulton, A.J., Painter, S.C., Young, J.R., Bates, N.R., Bowler, B., Drapeau, D., Lyczsckowski, E., Balch, W.M., 2013. The 2008 *Emiliania huxleyi* bloom along the Patagonian Shelf: ecology, biogeochemistry, and cellular calcification. Global Biogeochemical Cycles 27. http://dx.doi.org/10.1002/2013GB004641.

Poulton, A.J., Young, J.R., Bates, N.R., Balch, W.M., 2011. Biometry of detached *Emiliania huxleyi* coccoliths along the Patagonian Shelf. Marine Ecology Progress Series 443, 1–17. http://dx.doi.org/10.3354/meps09445.

Ramirez, F.C., 1970a. Copépodos planctónicos del sector bonaerense del Atlántico Sudoccidental. Informe Técnico Proyecto Desarrollo Pesquero (FAO-Argentina). Mar del Plata 10, 1–116.

Ramirez, F.C., 1970b. Copépodos planctónicos del sector patagónico. Resultados de la Campaña "Pesquería XI". Physics A 79, 473–476.

Ramirez, F.C., 1971. Copépodos planctónicos de los sectores bonaerenses y norpatagónicos. Resultados de la Campaña "Pesquería III". Revista del Museo La Plata (Nueva Serie). Sección Zoología 11, 73–94.

Ramirez, F.C., 1981. Zooplancton y producción secundaria. Parte I. Distribución y variación estacional de los copépodos. In: Angelescu, V. (Ed.), Campañas de investigación Pesquera realizadas en el Mar Argentino por los B/I "Shinkai Maru" y "Walther Herwig" y el B/P Marburg, años 1978 y 1979, N° 383. Serie Contribuciones INIDEP (Mar del Plata), pp. 202–212.

Ramirez, F.C., 2007. Distribución y alimentación del zooplankton. In: Carreto, J.I., Bremec, C. (Eds.), El Mar Argentino y sus recursos Pesqueros V: El ecosistema marino. Instituto Nacional de Investigación y Desarrollo Pesquero, Mar del Plata (Argentina), pp. 45–69.

Repeta, D.J., Gagosian, R.B., 1984. Transformation reactions and recycling of carotenoids and chlorins in the Peru upwelling region (15°S, 75 W). Geochimica et Cosmochimica Acta 48, 1265–1277.

Rijkenberg, M.J.A., Middag, R., Laan, P., Gerringa, L.J.A., van Aken, H.M., Schoemann, V., de Jong, J.T.M., de Baar, H.J.W., 2014. The distribution of dissolved Iron in the West Atlantic Ocean. PLoS ONE 9 (6), e101323. http://dx.doi.org/10.1371/journal.pone.0101323.

Rivas, A.L., Dogliotti, A.I., Gagliardini, D.A., 2006. Seasonal variability in satellite-measured surface chlorophyll in the Patagonian Shelf. Continental Shelf Research 26, 703–720.

Romero, S.I., Piola, A.R., Charo, M., Garcia, C.A.E., 2006. Chorophyll *a* variability off Patagonia based on SeaWiFS data. Journal of Geophysical Research 111, C05021.

Romero, O., Hensen, C., 2002. Oceanographic control of biogenic opal and diatoms in surface sediments of the Southwestern Atlantic. Marine Geology 186, 263–280.

Rynearson, T.A., Richardson, K., Lampitt, R.S., Sieracki, M.E., Poulton, A.J., Lyngsgaard, M.M., Perry, M.J., 2013. Major contribution of diatom resting spores to vertical flux in the sub-polar North Atlantic. Deep-Sea Research 182, 60–71.

Sabatini, M.E., Akselman, R., Reta, R., Negri, R.M., Lutz, V.A., Silva, R.I., Segura, V., Gil, M.N., Santinelli, N.H., Sastre, A.V., Daponte, M.C., Antali, J.C., 2012. Spring plankton communities in the southern Patagonian shelf: hydrography, mesozooplankton patterns and trophic relationships. Journal of Marine Systems 94, 35–51.

Salter, I., Kemp, A.E.S., Moore, C.M., Lampitt, R.S., Wolff, G.A., Holtvoeth, J., 2012. Diatom resting spore ecology drives enhanced carbon export from a naturally iron-fertilized bloom in the Southern Ocean. Global Biogeochemical Cycles 26, GB1014. http://dx.doi.org/10.1029/2010GB003977.

Saraceno, M., Provost, C., Piola, A.R., 2005. On the relationship of satellite retrieved surface temperature fronts and chlorophyll-*a* in the Western South Atlantic. Journal of Geophysical Research 110, C11016.

Sathyendranath, S., Platt, T., 1988. The spectral irradiance field at the surface and in the interior of the ocean: a model for applications in oceanography and remote sensing. Journal of Geophysical Research 93, 9270–9280.

Scherr, E.B., Scherr, B.F., 2007. Heterotrophic dinoflagellates: a significant component of microzooplankton biomass and major grazers of diatoms in the sea. Marine Ecology Progress Series 352, 187–197.

Scherr, E.B., Scherr, B.F., Ross, C., 2013. Microzooplankton grazing impact in the Bering Sea during spring sea ice. Deep Sea Research Part II 94, 57–67.

Schloss, I.R., Ferreyra, G.A., Ferrario, M.E., Almandoz, G.O., Codina, R., Bianchi, A.A., Balestrini, C.F., Ochoa, H.A., Ruiz-Pino, D., Poisson, A., 2007. Role of plankton communities in sea-air variations in pCO_2 in the SW Atlantic Ocean. Marine Ecology Progress Series 332, 93–106.

Segura, V., Lutz, V.A., Dogliotti, A., Silva, R.I., Negri, R.M., Akselman, R., Benavides, H., 2013. Phytoplankton types and primary production in the Argentine Sea. Marine Ecology Progress Series 491, 15–31.

Signorini, S.R., Garcia, V.M.T., Piola, A.R., Garcia, C.A.E., Mata, M., McClain, C.R., 2006. Seasonal and interannual variability of calcite in the vicinity of the Patagonian shelf break (38°S–52°S). Geophysical Research Letters 33, L16610. http://dx.doi.org/10.1029/2006GL026592.

Signorini, S.R., Garcia, V.T.M., Piola, A.R., Evangelista, M., McClain, C.R., Garcia, C.A.E., Mata, M.M., 2009. Further studies on the physical and biogeochemical causes for large interannual changes in the Patagonian shelf spring-summer phytoplankton bloom Biomass. NASA Technical Memorandum, NASA/TM-2009-214176, Greenbelt, MD, 43 pp.

Smayda, T.J., Trainer, V.L., 2010. Dinoflagellate blooms in upwelling systems: seeding, variability, and contrasts with diatom bloom behaviour. Progress in Oceanography 85 (1–2), 92–107.

Smyth, T.J., Allen, I., Atkinson, A., Bruun, J.T., Harmer, R.A., Pingree, R.D., Widdicombe, C.E., Somerfield, P.J., 2014. Ocean net heat flux influences seasonal to interannual patterns of plankton abundance. PLoS ONE 9 (6), e98709. http://dx.doi.org/10.1371/journal.pone.0098709.

Strub, P.T., James, C., Combes, V., Matano, R., Piola, A., Palma, E., Saraceno, M., Guerrero, R., Fenco, H., Ruiz Etcheverry, L., 2015. Altimeter-derived seasonal circulation on the Southwest Atlantic Shelf. Journal of Geophysical Research: Oceans 120 (5), 3391–3418. http://dx.doi.org/10.1002/2015JC010769.

Sugie, K., Kuma, K., Fujita, S., Ikeda, T., 2010. Increase in Si:N drawdown ratio due to resting spore formation by spring bloom-forming diatoms under Fe- and N-limited conditions in the Oyashio región. Journal of Experimental Marine Biology and Ecology 38 (2), 108–116.

Sverdrup, H.U., 1953. On conditions for the vernal blooming of phytoplankton. Journal du Conseil/Conseil Permanent International pour l'Exploration de la Mer 18, 287–295.

Szymczak-Zyla, M., Kowalewska, G., Louda, J.W., 2008. The influence of microorganisms on chlorophyll a degradation in the marine environment. Limnology and Oceanography 53, 851–862. http://dx.doi.org/10.4319/lo.2008.53.2.0851.

Takahashi, M., Seibert, D.L., Thomas, W.H., 1977. Occasional blooms of phytoplankton during summer in Saanich Inlet, B.C., Canada. Deep Sea Research 24, 775–780.

Taylor, J., Ferrari, R., 2011a. Shutdown of turbulent convection as a new criterion for the onset of spring phytoplankton blooms. Limnology and Oceanography 56, 2293–2307. http://dx.doi.org/10.4319/lo.2011.56.6.2293.

Taylor, J.R., Ferrari, R., 2011b. Ocean fronts trigger high latitude phytoplankton blooms. Geophysical Research Letters 38, L23601. http://dx.doi.org/10.1029/2011GL049312.

Townsend, D.W., Keller, M.D., Sieracki, M.E., Ackleson, S.G., 1992. Spring phytoplankton blooms in the absence of vertical water column stratification. Nature 360, 59–62. http://dx.doi.org/10.1038/360059a0.

Wadley, M.R., Jickells, D.T., Heywood, K.J., 2014. The role of iron sources and transport for Southern Ocean productivity. Deep Sea Research Part I 87, 82–94. http://dx.doi.org/10.1016/j. dsr.2014.02.003.

Walker, J.S., Keely, B.J., 2004. Distribution and significance of chlorophyll derivatives and oxidation products during the spring phytoplankton bloom in the Celtic Sea April 2002. Organic Geochemistry 35, 1289–1298. http://dx.doi.org/10.1016/j.orggeochem.2004.06.017.

Wang, J., Pierce, G.J., Sacau, M., Portela, J., Santos, M.B., Cardoso, X., Bellido, J.M., 2007. Remotely sensed local oceanic thermal features and their influence on the distribution of the hake (*Merluccius hubbsi*) at the Patagonian shelf edge in the SW Atlantic. Fisheries Research 83, 133–144.

Zamora-Terol, S., Nielsen, T.G., Saiz, E., 2013. Plankton community structure and role of *Oithona similis* on the western coast of Greenland during the winter-spring transition. Marine Ecology Progress Series 483, 85–102. http://dx.doi.org/10.3354/meps10288.

Zhang, Y., Lu, S., 2010. Distribution and germination of viable diatom resting stage cells in sediments of the East China Sea. Acta Oceanologica Sinica 29 (5), 121–128.

Zapata, M., Rodrıguez, F., Garrido, J.L., 2000. Separation of chlorophylls and carotenoids from marine phytoplankton: a new HPLC method using a reversed phase C8 column and pyridine-containing mobile phases. Marine Ecology Progress Series 195, 29–45.

Zapata, M., Jeffrey, S.W., Wright, S.W., Rodriguez, F., Garrido, J.L., Clementson, L., 2004. Photosynthetic pigments in 37 species (65 strains) of Haptophyta: implications for oceanography and chemotaxonomy. Marine Ecology Progress Series 270, 83–102.